Global and Planetary Change 196 (2021) 103373

Contents lists available at ScienceDirect

Global and Planetary Change

journal homepage: www.elsevier.com/locate/gloplacha

Decoupling $\delta^{13}C_{carb}$ and $\delta^{13}C_{org}$ at the onset of the Ireviken Carbon Isotope Excursion: $\Delta^{13}C$ and organic carbon burial (f_{org}) during a Silurian oceanic anoxic event

Emma R. Hartke [a,b], Bradley D. Cramer [a,*], Mikael Calner [c], Michael J. Melchin [d], Bruce A. Barnett [e], Stephan C. Oborny [f], Alyssa M. Bancroft [g]

[a] Department of Earth and Environmental Sciences, University of Iowa, Iowa City, IA 52242, USA
[b] Department of Geosciences, Pennsylvania State University, University Park, PA 16802, USA
[c] Department of Geology, Lund University, SE-223 62 Lund, Sweden
[d] Department of Earth Sciences, St. Francis Xavier University, Antigonish, NS B2G 2W5, Canada
[e] Department of Geology, University of Kansas, Lawrence, KS 66047, USA
[f] Kansas Geological Survey, University of Kansas, Lawrence, KS 66047, USA
[g] Indiana Geological and Water Survey, Indiana University, Bloomington, IN 47404, USA

A B S T R A C T

Paired records of $\delta^{13}C_{carb}$ and $\delta^{13}C_{org}$ across the Llandovery-Wenlock boundary demonstrate asynchronous behavior during the onset of the Ireviken Biogeochemical Event (IBE). The extremely high-resolution data produced from the Altajme Core, drilled from Gotland, Sweden, capture a negative excursion in $\delta^{13}C_{org}$ during the initiation of the Ireviken Extinction Event (IEE) and prior to the onset of the Ireviken positive $\delta^{13}C_{carb}$ Excursion (ICIE). The record of carbon isotopic changes through this interval illustrate that both $\Delta^{13}C$ (the difference between $\delta^{13}C_{carb}$ and $\delta^{13}C_{org}$) as well as the relative flux of organic carbon burial (f_{org}) vary in unique ways and at different times during the progression of the IBE. Both process-oriented variables within the global carbon cycle ($\Delta^{13}C$ and f_{org}) track a series of events that help to demonstrate potential causative mechanisms of both the extinction and carbon cycle perturbation. The sequence of events demonstrated here largely mirror the cascade of events that took place during the Cretaceous Oceanic Anoxic Event 2 (OAE2) and a detailed comparison between the two events is provided here for the first time. The unique insight into the IBE presented in this work results primarily from the novel, nearly Neogene-scale resolution of the paired isotope data, which demonstrates the critical importance of high-resolution chemostratigraphic research to evaluating ancient perturbations to the Earth-life system. Additional data sets of equal or greater resolution through this interval will be critical to evaluate the global synchroneity of these short-lived events during the IBE, and similar high-resolution studies of other Paleozoic biogeochemical events may shed light on potentially similar causative mechanisms.

1. Introduction

The stratigraphic record of biogeochemical cycling of carbon is a remarkable tool for tracking and interpreting important disruptions within the combined ocean-atmosphere-biosphere Earth system through geologic history. Past perturbations in the global carbon cycle can be reconstructed by studying changes in the isotopic composition of carbon in different geological materials through time. We recognize these shifts in the stable isotopic compositions of carbonate carbon ($\delta^{13}C_{carb}$) and organic carbon ($\delta^{13}C_{org}$) as they are preserved in sedimentary rocks as a proxy to understand how carbon was cycled within and among the rock reservoirs (organic- and carbonate-bearing rocks) and their interactions with the short-term carbon cycle of the ocean-atmosphere-biosphere (e.g. Berner, 1990; Kump and Arthur, 1999; Hayes et al., 1999; Cramer and Jarvis, 2020). These proxies are a sensitive tool useful for interpreting changes in both biotic and abiotic activity, such as primary productivity and sequestration or removal of carbon from the ocean and atmosphere (Berner, 1990; Hayes et al., 1999; Gruber et al., 1999; Ridgwell and Zeebe, 2005; Berner, 2006; Bachan et al., 2017; Cramer and Jarvis, 2020).

Major perturbations to the global carbon cycle are preserved in the rock record as carbon isotope excursions, identified when the carbon isotope value deviates from longer-term baseline values (e.g. Kump and Arthur, 1999; Cramer and Jarvis, 2020). The magnitude of these carbon isotope perturbations and whether their inflection is positive or negative implies a period of significant change to carbon cycling (Hayes et al., 1999; Kump and Arthur, 1999). Perturbations to the global carbon cycle occurred throughout geologic time, and many are well-studied and

* Corresponding author.
E-mail address: bradley-cramer@uiowa.edu (B.D. Cramer).

https://doi.org/10.1016/j.gloplacha.2020.103373
Received 15 July 2020; Received in revised form 2 November 2020; Accepted 3 November 2020
Available online 11 November 2020

identified in multiple sedimentary basins worldwide. Such is the case of the carbon isotope excursions of the Silurian Period (443–419 Ma, Melchin et al., 2020; Cramer and Jarvis, 2020). Extraordinary efforts to evaluate the Silurian carbon isotopic record during the past two decades have shown that this time period, in terms of global carbon cycling perturbations, is among the most dynamic intervals of Earth history and contains at least seven major positive carbonate-carbon isotope excursions (Samtleben et al., 1996; Hlad et al., 1997; Melchin and Holmden, 2006; Jeppsson et al., 2007; Kaljo et al., 2007; Munnecke et al., 2010; Cramer et al., 2011; Racki et al., 2012; McLaughlin et al., 2013; Frýda and Štorch, 2014; Radzevičius et al., 2014; Kaljo et al., 2015; Kozłowski, 2015; Sullivan et al., 2016; Waid and Cramer, 2017; McAdams et al., 2017; Danielsen et al., 2019; McAdams et al., 2019; Oborny et al., 2020; Cramer and Jarvis, 2020).

In order to facilitate clear differentiation in our discussion between the series of events that took place across the Llandovery-Wenlock boundary, we use the term Ireviken Extinction Event (IEE) to discuss the biotic turnover first identified by Jeppsson (1987) and use this term separately from Ireviken Carbon Isotope Excursion (ICIE), to refer exclusively to the positive carbonate-carbon isotope excursion, or the Ireviken Biogeochemical Event (IBE) as the sum of all these (see Cramer et al., 2010). The IBE that spans the Llandovery-Wenlock boundary (~432 Ma, Cramer et al., 2012; Melchin et al., 2020) is the best-studied biogeochemical event of the Silurian, and has been identified in more than two dozen localities world-wide (e.g., Jeppsson et al., 1995; Jeppsson, 1997; Cramer et al., 2010; Bancroft and Cramer, 2020). The IBE is associated with both a major marine extinction event (IEE) and a significant perturbation to the global carbon cycle (ICIE). The extinction interval (IEE) spans the Llandovery-Wenlock boundary (Jeppsson, 1997; Cramer et al., 2010), and the "onset" of the positive carbon isotope excursion (ICIE) begins just above the boundary and extends well into the Sheinwoodian Stage (~432–430 Ma; see Cramer et al., 2010; McAdams et al., 2019; Melchin et al., 2020; Cramer and Jarvis, 2020). The extinction severely impacted conodont and trilobite species globally while simultaneously impacting graptolites, brachiopods, corals, ostracodes, and polychaetes (Jeppsson, 1987; Jeppsson, 1990; Calner et al., 2004; Calner, 2008; Cramer et al., 2010; Cooper et al., 2014; Crampton et al., 2016). The ICIE typically reaches values > +5.0‰ before returning to baseline within the middle part of the Sheinwoodian Stage (e.g. Cramer et al., 2010; Melchin et al., 2020; Cramer and Jarvis, 2020).

The overwhelming majority of carbon isotope studies of the IBE have focused exclusively on carbonate carbon, with only a handful of recent studies including paired carbon isotope data (Cramer and Saltzman, 2007a; Richardson et al., 2019; Rose et al., 2019; Young et al., 2019). When organic carbon isotope samples have been produced, they are frequently provided without paired carbonate carbon isotope data (e.g., Loydell and Frýda, 2007; Frýda and Štorch, 2014), which has limited our ability to directly compare the two carbon isotope records and fully evaluate the global carbon cycle during this event. In this study, we produced paired organic and carbonate carbon isotope samples ($\delta^{13}C_{org}$ and $\delta^{13}C_{carb}$) at exceptionally high resolution from a single core from the Swedish island of Gotland, located in the Baltic Sea (Fig. 1) that was drilled specifically for this investigation. The ~350 m-long Altajme Core spans an interval from the Hirnantian Stage of the Ordovician System (~444 Ma, Gradstein et al., 2020) through the Homerian Stage of the Silurian System (~427 Ma, Gradstein et al., 2020). Here, we focused on a 132-m interval spanning the Llandovery-Wenlock boundary.

2. Geological setting

Strata on Gotland are fossiliferous, exceptionally preserved, largely free of diagenetic alteration, devoid of tectonic disturbance, and well constrained by biostratigraphy, ranging in age from late Llandovery to Ludlow (e.g., Samtleben et al., 1996; Calner et al., 2004; Jeppsson et al., 2006). The exposed Silurian succession on Gotland is >700 m thick and was deposited between a latitude of 10° and 20° south (Fig. 1). The tropical latitude and the distance from clastic sources promoted extensive carbonate development on Gotland throughout much of the Silurian. The lithostratigraphic interval studied here includes the Lower

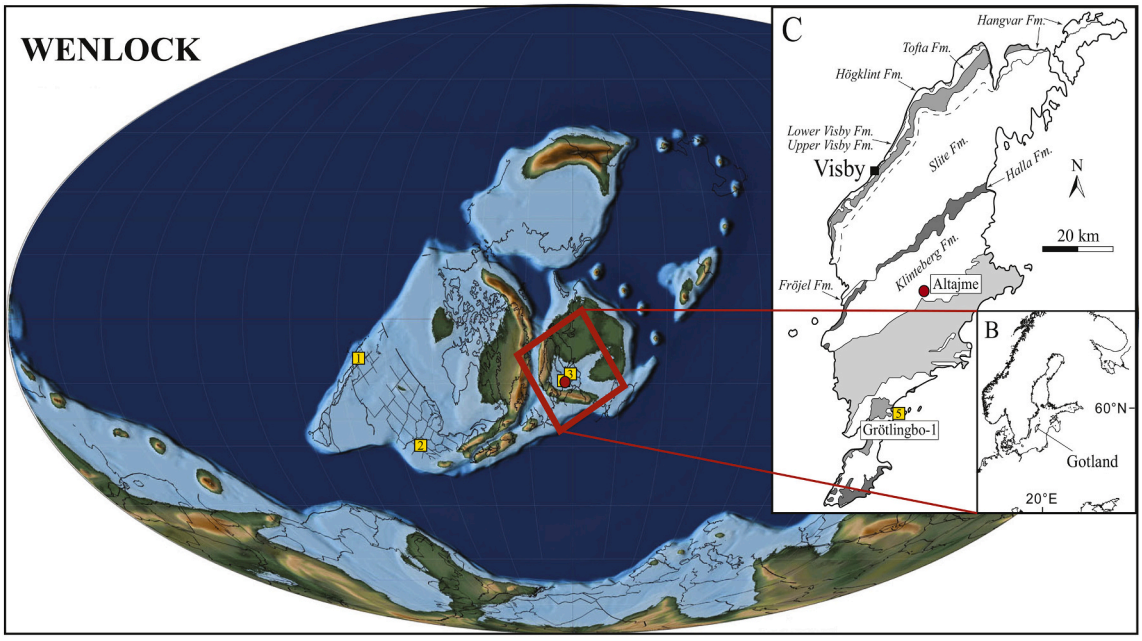

Fig. 1. A) Wenlock Paleogeography (Scotese, 2014). Red circle indicates location of Altajme Core, Gotland, Sweden. Yellow boxes indicate location of other paried carbon isotope data sets discussed in the text. 1 – Nevada, Young et al. (2019), 2 – Tennessee – Cramer and Saltzman, 2007a, 3 – Estonia – Richardson et al. (2019), 4 (hidden behind red dot in Panel A) – Gotland, Rose et al. (2019). B) Inset map showing location of Gotland, Sweden, in the present-day Baltic Sea. C) Inset geologic map of Gotland, Sweden (modified from Cramer et al., 2012) showing lithostratigraphic units discussed in text as well as locations of the Altajme and Grötlingbo-1 drill cores. 5 - Grötlingbo-1 – Männik et al. (2015). (For interpretation of the references to colour in this figure legend, the reader is referred to the web version of this article.)

Visby, Upper Visby, Högklint, Tofta, and Hangvar formations, and overlying Slite Group (see Calner et al., 2004; Jeppsson et al., 2006). The location of the Altajme Core, which was drilled at the abandoned Altajme quarries ca 2200 m southwest of Buttle Church in south-central Gotland (Fig. 1), is considerably removed from the outcrop belt that contains the Llandovery-Wenlock boundary interval in the northwest of the island. As a result, the typically reefal lithologies of the Högklint and Tofta formations are considerably less calcareous in the core and more organic rich, which enables continuous sampling for both $\delta^{13}C_{carb}$ and $\delta^{13}C_{org}$ throughout the interval.

The IBE spans the Llandovery-Wenlock boundary and persisted for more than 1 Myr from the beginning of the extinction event (IEE) to the end of the carbon isotope excursion (ICIE) (Cramer et al., 2010; Melchin et al., 2020; Cramer and Jarvis, 2020). The onset of the IEE began during the latest Llandovery and persisted into the earliest Wenlock (Jeppsson, 1987, 1997; Cramer et al., 2010; Melchin et al., 2020), whereas the ICIE began within the extinction interval (Munnecke et al., 2003; Cramer et al., 2010) and extended into the middle part of the Sheinwoodian Stage of the Wenlock Series (Fig. 2). The extinction event was originally identified as a series of "extinction datums" by Jeppsson (1987) ranging from Datum 1 to Datum 8. Current correlations place the basal Wenlock (base Sheinwoodian) Global Boundary Stratotype Section and Point (GSSP) essentially at Datum 2 of the IEE (see discussions in Cramer et al., 2010; Melchin et al., 2020). The onset of the ICIE has been well documented on Gotland to coincide with Datum 4 (Munnecke et al., 2003), which is also the position of the boundary between the Lower and Upper Visby formations. The extinction interval ends within the ascending limb of the $\delta^{13}C_{carb}$ excursion and elevated carbon isotope values persist well after the extinction interval. Biostratigraphic data are still being compiled for the Altajme Core. However, litho- and chemostratigraphic data, and preliminary graptolite identifications from the core (combined with preexisting biostratigraphic data from the southern Gotland Grotlingbo-1 Core; Männik et al., 2015) permit the identifications of lithostratigraphic units; typically down to the level of individual beds found throughout the outcrop belt. A series of volcanic ashes, preserved as K-bentonites, are present in the Gotland succession and several important potassium (K)-bentonites can be identified in the Altajme Core. Specifically, a series of three bentonites (Ireviken, Störbrut, and Lusklint) occur near the Lower Visby/Upper Visby contact on Gotland (e.g., Batchelor and Jeppsson, 1994; Jeppsson, 1997; Kiipli et al., 2001; Cramer et al., 2012) and a series of three bentonites occur in a similar position in the Altajme Core (Appendix Fig. A1), which provides additional chronostratigraphic correlation with the outcrop belt on Gotland. More K-bentonites occur below this interval in the Altajme Core, and until further geochemical analysis of each K-bentonite layer can be conducted (e.g., Kiipli et al., 2001), the identification of the three K-bentonites in the Altajme Core will remain tentative.

3. Methods

For this project we collected 882 $\delta^{13}C_{carb}$ samples at 15 cm spacing and 265 $\delta^{13}C_{org}$ at 50 cm spacing to produce the highest resolution record ever recovered for this interval. Individual samples were powdered using a tungsten carbide drill bit attached to a hand drill with special attention paid to avoid sampling fossils or obvious diagenetic alteration such as secondary calcite (Cramer and Jarvis, 2020). Upon producing approximately 2 g of powder, a split of ~100 mg was taken for $\delta^{13}C_{carb}$ analysis and approximately 1 g of powder was separated for $\delta^{13}C_{org}$ analysis. Decarbonatization of $\delta^{13}C_{org}$ samples was carried out in 50 mL centrifuge tubes through the addition of 20 mL of 0.5 M HCl in three successive steps for a total of 60 mL per sample. After each 20 mL acid wash we spun the samples in a centrifuge to separate the solid and liquid components and decanted the waste acid from each sample before repeating this process for a total of three acid washes per sample. Some samples were sufficiently carbonate rich they required a fourth acid wash to complete decarbonatization. We followed this process by completing three water washes with de-ionized (DI) water to ensure all HCl was rinsed from each sample. The water wash procedure followed the same steps as that of the acid washes for a total of 60 mL of DI water. Samples were placed in a 40 °C oven for two to three days to ensure

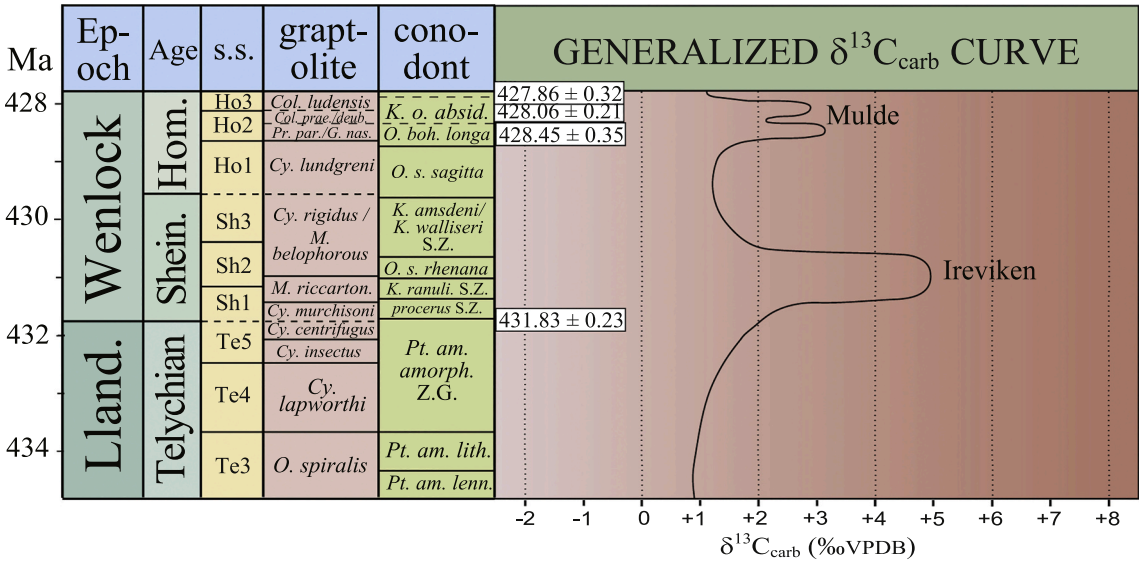

Fig. 2. Geologic time scale of the Silurian across the Llandovery-Wenlock boundary with respective conodont and graptolite biozones and a generalized $\delta^{13}C_{carb}$ curve (McAdams et al., 2019). Numerical ages for zonal and stage boundaries differ between GTS 2012 (Melchin et al., 2012), the GSA v.5 Timescale (Walker et al., 2018), the compilation of McAdams et al. (2019), and the newly released GTS 2020 (Melchin et al., 2020). The discrepancies around the Llandovery-Wenlock boundary are discussed in detail in Melchin et al. (2020). The radioisotopic date shown at the Llandovery-Wenlock boundary in this figure is from Cramer et al. (2012) from the Ireviken Bentonite on Gotland and serves as a direct date from the stratigraphy included here. Abbreviations: Lland. = Llandovery, Shein. = Sheinwoodian, Hom. = Homerian, S.S. = Stage Slice (Cramer et al., 2011), GRAPTOLITES: *O.* = *Oktavites*, *Cy.* = *Cyrtograptus*, *M.* = *Monograptus*, *Pr.* = *Prybilograptus*, *Col.* = *Colonograptus*, CONODONTS: *Pt.* = *Pterospathodus*, *am.* = *amorphognathoides*, *lenn.* = *lennarti*, *lith.* = *lithuanicus*, *amorph.* = *amorphognathoides*, Z.G. = Zonal Group, *procerus* = *Pterospathodus pennatus procerus*, S.Z. = Super Zone, *K.* = *Kockelella*, *ranuli.* = *ranuliformis*, *O.* = *Ozarkodina*, *s.* = *sagitta*, *boh.* = *bohemica*, *o.* = *ortus*. Names of excursions follow Cramer et al. (2011), also see discussion in Melchin et al. (2020).

complete drying of the samples before grinding with an agate mortar and pestle followed by cleaning with ethanol between each sample. Both carbonate and organic carbon samples were sent to the Keck Paleoenvironmental and Environmental Stable Isotope Laboratory (KPESIL) at the University of Kansas for analysis and all data are available online (Appendix A, Table A1).

3.1. Carbonate carbon

Carbonate powders were reacted with 100% phosphoric acid with density > 1.9 (Wachter and Hayes, 1985) via a KIEL Carbonate Device connected to a ThermoFinnegan MAT 253 isotope ratio mass spectrometer. Sample $\delta^{13}C_{carb}$ and $\delta^{18}O_{carb}$ values were calibrated relative to the VPDB scale using internationally accepted (primary) standards NBS-18 and NBS-19, and daily performance monitored using laboratory established (secondary) standards TSF-1, SIGMA CALCITE, and 88b Dolomite analyzed at the beginning, middle and end of each 40 sample queue. Runs were stopped if the second standard ^{18}O value (always NBS-18) was more than 0.17‰ off (the known uncertainty of ^{18}O of NBS-18). The carbonate system is calibrated utilizing both NBS-18 and NBS-19 due to known variability when utilizing microgram quantities of NBS-19, which is granular (typically fine sand to coarse-sized silt). The precision of both carbon and oxygen was better than 0.10‰ for all samples analyzed. Carbonate content was determined via weighing the sample prior to, and following, decarbonatization, but before removal from the sample tube and pulverization. The weight percent digested at this step was taken as carbonate weight percent.

3.2. Organic carbon

Samples were weighed and wrapped in 5 × 9 mm pressed tin capsules and loaded into a Costech Zero Blank Autosampler, after which the samples and resulting gases were under continuous flow from an Ultrapure Helium gas stream. Samples were combusted with an aliquot of

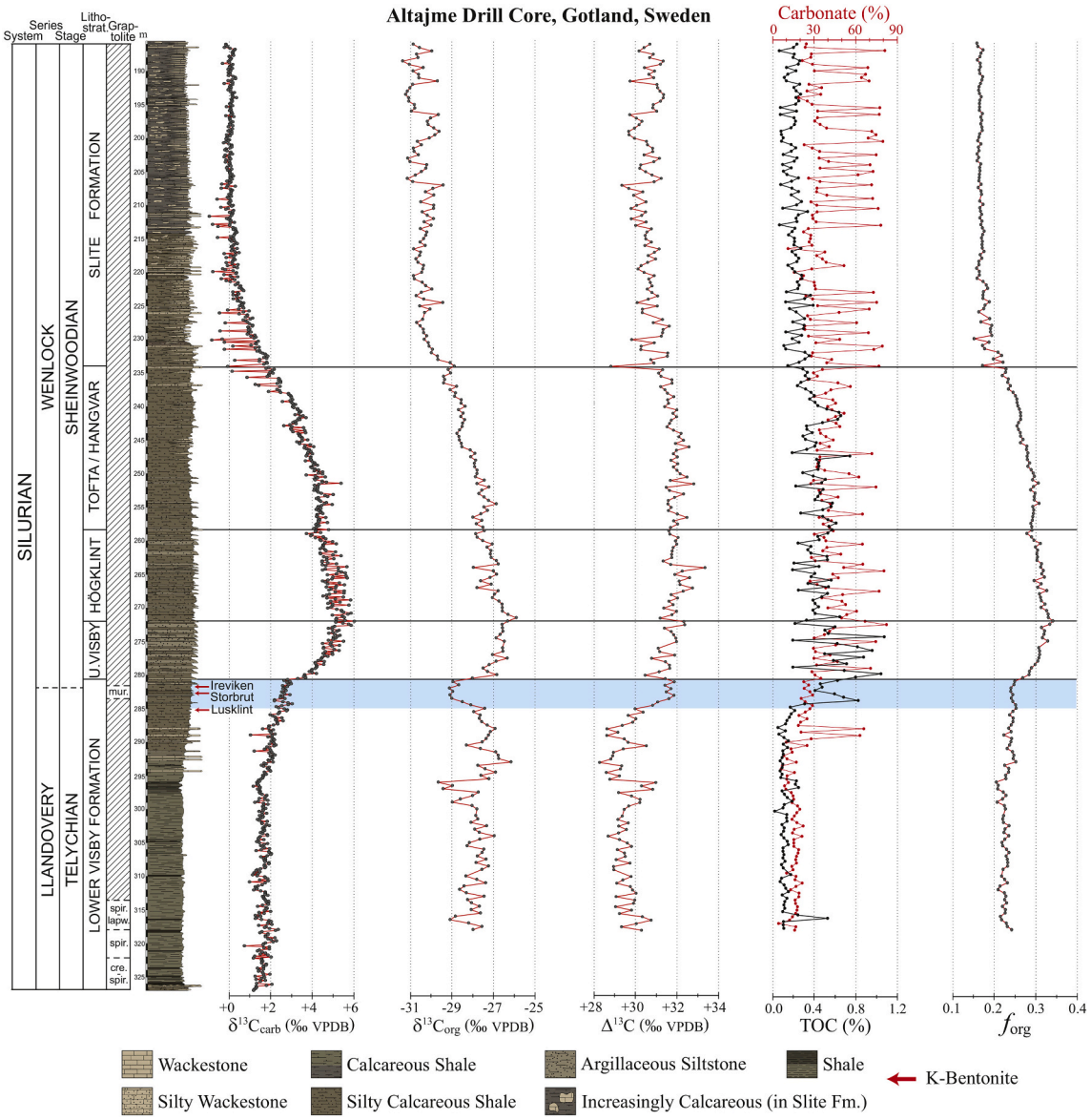

Fig. 3. Stratigraphic section of the Altajme drill core showing from left to right, $\delta^{13}C_{carb}$, $\delta^{13}C_{org}$, and $\Delta^{13}C$ (in ‰ VPDB), (TOC) and carbonate (in %), and the calculated f_{org} (percentage of all carbon burial that is organic carbon, see text for discussion). The highlighted region in the blue box indicates the onset of the Ireviken Biogeochemical Event (IBE), identified here as the onset of the negative excursion in $\delta^{13}C_{org}$. Abbreviations: cre.-spir. = either *Monoclimacis crenulata* or *Oktavites spiralis* zone, spir. = *Oktavites spiralis* zone, spir.-lapw. = either *Oktavites spiralis* or *Cyrtograptus lapworthi* zone. (For interpretation of the references to colour in this figure legend, the reader is referred to the web version of this article.)

oxygen in a Costech Instruments ECS 4010 (Elemental Combustion System). The combustion furnace was maintained at 980 °C, however ultimate combustion temperature was between 1700 °C and 1800 °C owing to the addition of oxygen and tin. Excess oxygen and nitrous compounds were reduced in the reduction furnace maintained at 600 °C. Water was removed with a magnesium perchlorate trap, CO_2 and N_2 gases were separated in a GC Column maintained at 50 °C. Separated gases were interfaced via a Thermo Finnigan Conflo III for introduction to a Thermo Finnigan MAT 253 Stable Isotope Mass Spectrometer. Samples were analyzed with a suite of both primary and secondary (laboratory) stable isotope standards including USGS-24, ANU, and IAEA-600. The precision for organic carbon isotope analysis was better than 0.11‰ for all analyses. Total organic carbon was determined by establishing the linear relationship between peak area of mass 44 (CO_2) as measured with the isotope ratio mass spectrometer and carbon content. During each analysis several standards of known carbon content were measured resulting in a linear regression ($R^2 > 0.99$) used to calculate sample carbon content from sample mass 44 areas. The TOC content of each organic carbon sample was then calculated against the original sample weight of each sample prior to decarbonatization to provide the reported TOC value listed in Table A1 and shown in Fig. 3.

4. Results

4.1. Carbonate carbon

Much of the Lower Visby Formation sampled herein maintains baseline $\delta^{13}C_{carb}$ values between +1‰ and +2‰. Values increase slightly within the upper seven meters to near +3‰ (Fig. 3). At the boundary between the Lower and Upper Visby formations (280.55 m) $\delta^{13}C_{carb}$ values begin to increase rapidly from +3‰ to just above +6‰ at 272 m near the Upper Visby/Högklint contact. The inflection point of most rapid positive change in $\delta^{13}C_{carb}$ (i.e., onset of the ICIE, see discussion in Cramer et al., 2010) is well identified on Gotland (e.g. Munnecke et al., 2003; Cramer et al., 2010) and is coincident with both Datum 4 of the IEE (Jeppsson, 1997) and the Lower/Upper Visby contact. Carbonate carbon isotope values remain between +4‰ and +6‰ throughout most of the Högklint Formation. In the Altajme Core, it was difficult to identify the boundary between the Tofta and the Hangvar formations, so they are herein grouped as a single unit (Fig. 3). However, this boundary may be located at 243 m where a slight color change was observed accompanied by staining and discoloration. $\delta^{13}C_{carb}$ values remain above +4‰ for approximately the lower half of this undifferentiated interval before descending to values of +2‰ at the contact with the overlying Slite Formation. Values continue to decline in the lowermost part of the Slite Formation until reaching a mid-Wenlock baseline of ~0‰ at around 220 m.

With the exception of two samples (Fig. 3), the Lower Visby Formation is exclusively below 30% carbonate, which is uniquely set apart from the remainder of the core. In general, the stratigraphic units that contain the ICIE (Upper Visby, Högklint, Tofta, Hangvar) have higher carbonate content than do the units above or below the excursion, which has been a long-identified feature of Gotland chemostratigraphy (Jeppsson, 1990; Samtleben et al., 1996; Munnecke et al., 2003). All data are shown with TOC and carbonate % in separate columns in Appendix Fig. A4.

4.2. Organic carbon

Organic carbon isotope values are between −29‰ and −27‰ throughout most of the Lower Visby Formation with an average value near −28‰ (Fig. 3). A slight negative inflection occurs around the 297 m position before abruptly increasing to approximately −27‰ at 295 m. Values remain around −27‰ until 288 m at which point $\delta^{13}C_{org}$ values decline to −29‰ in the uppermost part of the formation. Values rapidly increase to above −27‰ across the Lower Visby/Upper Visby contact. $\delta^{13}C_{org}$ values continue to increase throughout the Upper Visby and reach their highest values, above −26‰, within the lowest part of the Högklint Formation. From this position $\delta^{13}C_{org}$ values generally track $\delta^{13}C_{carb}$ values during the long decline back to baseline values within the lower part of the Slite Formation at approximately −30‰.

Total Organic Carbon (TOC) values for the majority of the core are below 1.0%, with the exception of two samples in the Upper Visby Formation. TOC values are generally below 0.2% for most of the Lower Visby before an initial increase above 0.2% between approximately 288 m and 285 m. In the remaining ~5 m of the uppermost part of the Lower Visby Formation (above 285 m), TOC values increase rapidly and are all above 0.4%, coincident with the transient low in $\delta^{13}C_{org}$ values. The overlying Upper Visby records the highest TOC values that approach 0.8% as an average, and the Högklint through Tofta/Hangvar interval hover around 0.4% TOC. Above the ICIE, TOC values return to an apparent baseline in the core of approximately 0.2%. To illustrate that $\delta^{13}C_{org}$ values are not exclusively responding to the amount of organic carbon present in each sample throughout the core we illustrate the relationship between $\delta^{13}C_{org}$ and TOC (Fig. 4). The calculated R^2 value for their relationship is 0.0906, which highlights the fact that $\delta^{13}C_{org}$ in the Altajme Core is independent of TOC.

4.3. Biostratigraphy

The graptolites investigated for this study occur in three main stratigraphic intervals: between 281.21 and 283.47 m; at 296.69 m; and between 309.85 and 326.12 m (Fig. 3). The graptolites occur as flattened to low relief specimens on bedding planes. At this point no attempt has been made to extract graptolites by acid dissolution. Preliminary study of the graptolite faunas shows that the entire studied interval ranges in age from mid-upper Telychian into the Llandovery-Wenlock boundary interval of the *Cyrtograptus murchisoni* Biozone (Figs. 2 and 3). *Monograptus priodon* and *Retiolites angustidens* are the two most commonly occurring species and they are present throughout most of the studied interval. Both of these taxa range in age from the mid-late Telychian, below the base of the *Oktavites spiralis* Biozone, into the upper part of the *C. murchisoni* Biozone, in the lower Wenlock (Loydell et al., 2008; Zalasiewicz et al., 2009).

The most age-diagnostic graptolite faunas occur in two intervals. The

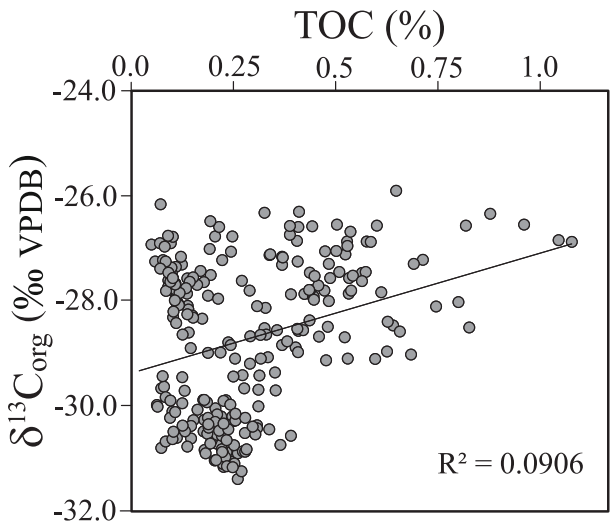

Fig. 4. Comparison between $\delta^{13}C_{org}$ and TOC to illustrate that $\delta^{13}C_{org}$ values obtained from this study are independent of TOC. A strong correlation between $\delta^{13}C_{org}$ and TOC (e.g., a high R^2 value) would suggest that the $\delta^{13}C_{org}$ record were primarily driven by how much TOC was available to be measured in each sample, and therefore not likely to be recording meaningful values from the Silurian sedimentary record.

lower of these two intervals begins at 322.14 m, the level of the first appearance of *Oktavites spiralis*, indicative of the *O. spiralis* Biozone. Several of the samples below this level contain *Monograptus parapriodon*, which is common in the *O. spiralis* Biozone but also appears elsewhere in the upper part of the underlying *Monoclimacis crenulata* Biozone (e.g., Loydell et al., 2008). Specimens of species of *Monoclimacis* also occur in this lower interval, but this material requires further study. Thus, the samples between 326.12 and 322.14 m could belong to the *O. spiralis* or the *M. crenulata* Biozone.

The highest sample indicative of the *O. spiralis* Biozone occurs at 316.00 m and it contains *Monograptus parapriodon*. Although this species has been reported from higher strata in North America (Lenz, 1982; Melchin, 1989) those specimens are significantly wider than the type material and the other reported occurrences of this species in Europe, which occur no higher than the *O. spiralis* Biozone (e.g., Štorch, 1994a; Loydell et al., 2008; Zalasiewicz et al., 2009). The stratigraphically higher Canadian material may represent a different species.

The occurrence of *Streptograptus* cf. *speciosus* at 313.57 m may be indicative of the *O. spiralis* or *Cyrtograptus lapworthi* biozones. The samples between 310.03 and 296.68 m contain only *Monograptus priodon* and are, therefore, not age-diagnostic for this interval.

The 283.47 m sample contains *Mediograptus vittatus*, a species known only to occur in the *Cyrtograptus murchisoni* Biozone (Štorch, 1994b; Männik et al., 2015). The samples above this level to 281.62 m contain taxa consistent with a level no higher than the *C. murchisoni* Biozone, including *M. priodon*, *R. angustidens*, and a single fragmentary specimen of *Cyrtograptus* sp. A complete biostratigraphic analysis of the entire core is currently underway for both conodont and graptolite biostratigraphy that will provide additional detail beyond the initial identifications and zonation included here, including photographic and museum accession documentation of all specimens.

5. Discussion

The results presented here are the highest resolution paired $\delta^{13}C_{org}$ with $\delta^{13}C_{carb}$ dataset ever produced for the Ireviken positive carbon

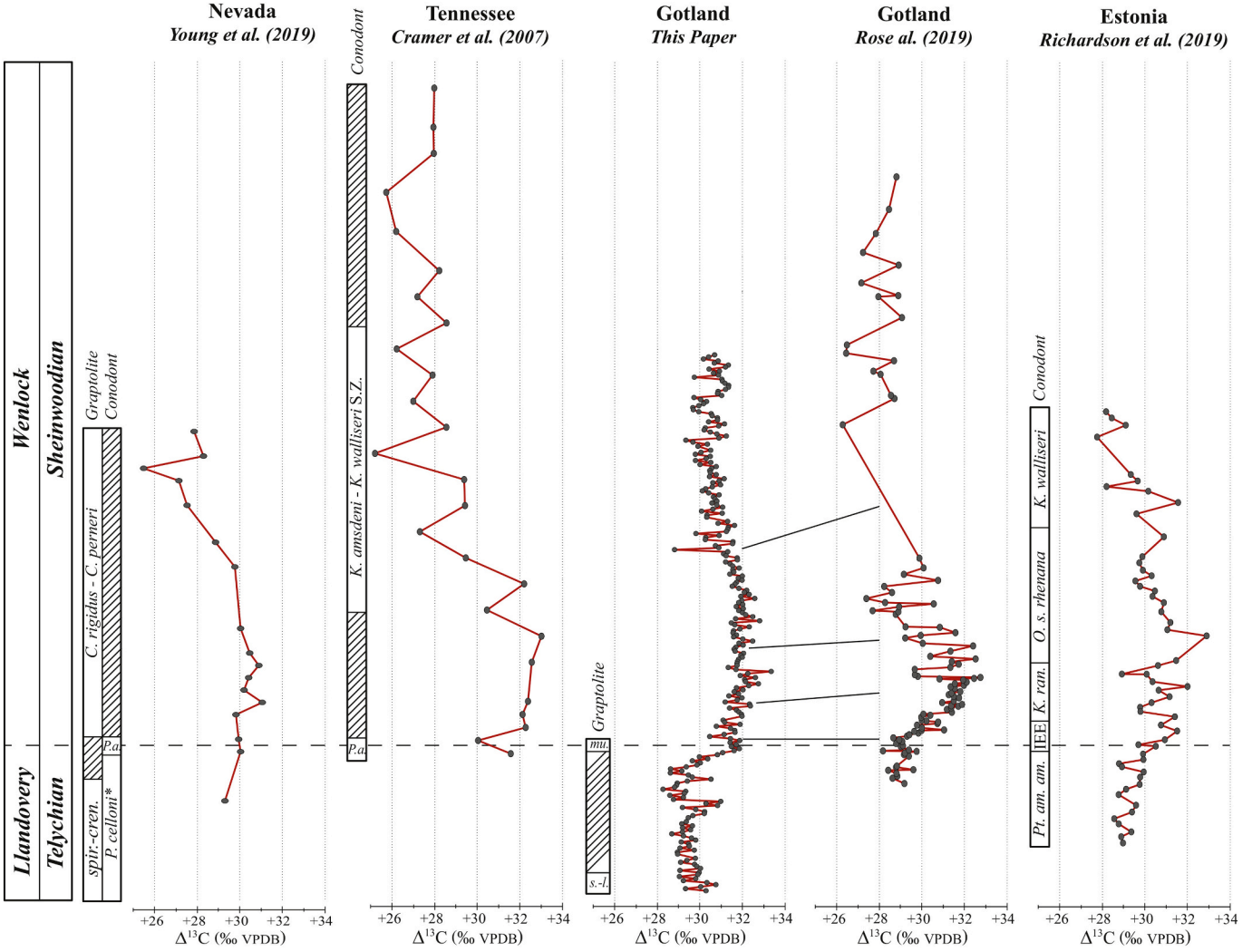

Fig. 5. Comparison of published $\Delta^{13}C$ records from Nevada (Young et al., 2019), Tennessee (Cramer and Saltzman, 2007a), this report, Gotland (Rose et al., 2019), and Estonia (Richardson et al., 2019). Note the general agreement in values for $\Delta^{13}C$ before, during, and after the ICIE. Solid black lines between the column for the Altajme Core (this paper) and the data from Rose et al. (2019) are tentative correlations based upon formation boundaries. It is difficult to evaluate or reconstruct the stratigraphic section for Gotland those authors utilized (e.g., how they interpreted their sections to overlap) based upon the limited outcrop locality and position information provided their report, and the correlations presented here remain tentative. Biozonations from original publications shown for Nevada and Estonia. Zonation updated for Tennessee to match zonation shown in Fig. 2 of this paper. Abbreviations: spir.-cren. = either *Oktavites spiralis* zone or *Monoclimacis crenulata* zone, *C.* = *Crytograptus*, *P.* = *Pterospathodus*, *a.* = *amorphognathoides*, *K.* = *Kockelella*, S.Z. = Super Zone, *s.-l.* = either *Oktavites spiralis* zone or *Cyrtograptus lapworthi* zone, *mu.* = *Cyrtograptus murchisoni* zone, *Pt. am. am.* = *Pterospathodus amorphognathoides amorphognathoides*, IEE = Ireviken Extinction Event, *ran.* = *ranuliformis*, *O. s. rhenana* = *Ozarkodina sagitta rhenana*. (For interpretation of the references to colour in this figure legend, the reader is referred to the web version of this article.)

isotope excursion interval and they demonstrate potential driving mechanisms for the ICIE as well as an unusual decoupling of the $\delta^{13}C_{carb}$ and $\delta^{13}C_{org}$ records immediately before the onset of the ICIE. $\Delta^{13}C$ values, the difference between carbonate and organic carbon isotope values, calculated as $\delta^{13}C_{carb}$ - $\delta^{13}C_{org}$, rise by +2‰ prior to the onset of $\delta^{13}C_{carb}$ increase due to a rapid transient negative excursion in $\delta^{13}C_{org}$ while $\delta^{13}C_{carb}$ was slightly increasing (immediately prior to the ICIE, blue box in Fig. 3). This is then followed by an additional interval of elevated $\Delta^{13}C$ where both $\delta^{13}C_{org}$ and $\delta^{13}C_{carb}$ exhibit a positive excursion (during the ICIE).

Transient changes in $\Delta^{13}C$ are significant in that both $\delta^{13}C_{carb}$ and $\delta^{13}C_{org}$ records are broadly expected to follow the same overall trends, and any variation between them (i.e., a change in $\Delta^{13}C$) indicates a perturbation to the global carbon cycle (see Hayes et al., 1999; Kump and Arthur, 1999; and discussion below). This decoupling between $\delta^{13}C_{carb}$ and $\delta^{13}C_{org}$ within the IEE has never been identified with paired sample sets and is likely visible here for the first time due to the resolution provided. However, a negative excursion in $\delta^{13}C_{org}$ from Gotland was identified by Vandenbroucke et al. (2013) from this precise interval and that report was the first indication of this feature (blue box in Fig. 3). The overall increase in $\Delta^{13}C$ during the ICIE (positive excursion above the blue box in Fig. 3) has been documented previously in datasets from the eastern margin of the Panthalassic Ocean (Nevada – Young et al., 2019), eastern margin of the Illinois Basin (Tennessee – Cramer and Saltzman, 2007a), and the Baltic Basin (Gotland – Rose et al., 2019; Estonia – Richardson et al., 2019). Comparison of these data sets with the new information provided here (Fig. 5) demonstrates a fairly consistent record of a 2–3‰ increase in $\Delta^{13}C$ during the IBE with values of 28–29‰ prior to the IBE and 31–32‰ during the IBE across all three basins.

Whereas several examples of decoupling between $\delta^{13}C_{org}$ and $\delta^{13}C_{carb}$ have been illustrated throughout the Phanerozoic (e.g., Patzkowsky et al., 1997; Kump et al., 1999; Kump and Arthur, 1999; Saltzman et al., 2011), the precise mechanism(s) behind these variations remain poorly understood. Here, we utilize the relationships between components of the global carbon cycle (e.g., Hayes et al., 1999; Berner, 2006) to discuss this initial decoupling of $\delta^{13}C_{org}$ and $\delta^{13}C_{carb}$ records during the onset of the IEE as well as the possible drivers of the overall changes in $\Delta^{13}C$ during the ICIE. It is important to recognize that there are two intervals with elevated $\Delta^{13}C$ that likely have different causal mechanisms. The initially decoupled interval during the IEE (blue box in Fig. 3) where steady or slightly increasing $\delta^{13}C_{carb}$ values coincide with a negative excursion in $\delta^{13}C_{org}$, and a second interval during the ICIE where both $\delta^{13}C_{carb}$ and $\delta^{13}C_{org}$ records show a positive excursion but the total change in $\delta^{13}C_{carb}$ slightly exceeds that of $\delta^{13}C_{org}$.

5.1. Isotope mass balance

Photosynthesis imparts a large fractionation of carbon due to the preferential uptake of ^{12}C by organic matter, such that typical marine organic carbon is highly enriched in ^{12}C compared to ^{13}C. Partitioning of ^{12}C from the ocean-atmosphere into the lithosphere during organic carbon burial therefore results in a net increase in the $^{13}C/^{12}C$ ratio (i.e., $\delta^{13}C$) of the remaining carbon pool in the ocean-atmosphere (Falkowski, 2003; Ciais et al., 2013; Cramer and Jarvis, 2020) that can be preserved in the rock record as a positive $\delta^{13}C$ excursion. From a mass balance perspective (Hayes et al., 1999; Berner, 2006), where the total amount of carbon being fluxed to the ocean-atmosphere from the lithosphere must equal the total amount of carbon being fluxed to the lithosphere from the ocean-atmosphere, and where the total amount of ^{13}C must also be equal for these fluxes, the isotopic composition of components of the global carbon cycle can be written as Eq. (1):

$$\delta^{13}C_{carb} = \delta^{13}C_{incoming} + f_{org}(\Delta^{13}C) \quad (1)$$

where $\delta^{13}C_{carb}$ and $\delta^{13}C_{incoming}$ are the carbon isotope values of carbonate carbon and carbon being fluxed from the lithosphere, respectively, and f_{org} is the fraction of all carbon burial that is organic.

From the Altajme Core we measured $\delta^{13}C_{carb}$ as well as $\Delta^{13}C$, which allow us to evaluate prior hypotheses of increased organic carbon burial (increased f_{org}) as a driver for the Ireviken Excursion (e.g., Munnecke et al., 2003; Cramer and Saltzman, 2005, 2007b), the results of which are shown in Fig. 3 and summarized in Table 1. For the interval prior to the onset of the $\delta^{13}C_{carb}$ excursion (defined here as the point of maximum rate of positive change, Cramer et al., 2010), $\delta^{13}C_{carb}$ is approximately +1.5‰ and $\Delta^{13}C$ is approximately +29.5‰. Utilizing a value of −5.0‰ for $\delta^{13}C_{incoming}$ (Derry and France-Lanord, 1996; Hayes et al., 1999; Berner, 2006), we calculate an initial f_{org} value of 0.22, which is similar to the modern-day value of 0.20 (Shackleton and Hall, 1984; Shackleton, 1987). During the onset of the IBE (blue bar in Fig. 3), f_{org} only rises to 0.24 which represents a ~9% increase in organic carbon burial from pre-event values. However, during the highest $\delta^{13}C_{carb}$ values at the "peak" of the positive carbon isotope excursion (lower part of the Högklint Formation) f_{org} increases to over 0.31 indicating an increase of at least 40% in organic carbon burial. Whereas this does not conclusively demonstrate that increased organic carbon burial was the only possible cause of the ICIE, it does demonstrate that such a hypothesis is consistent with the new data presented herein. This interpretation of the apparent increase in f_{org} as a demonstration of increased organic carbon burial as the ultimate driver of the ICIE is also consistent with recent $\delta^{34}S$ evidence of expanded euxinia during the early Sheinwoodian (e.g., Young et al., 2019; Rose et al., 2019; Richardson et al., 2019), which would have had the effect of promoting burial of organic carbon in expanded reducing environments.

The interval immediately prior to the onset of the ICIE shows a decoupled carbon record where $\delta^{13}C_{carb}$ was slightly increasing yet $\delta^{13}C_{org}$ was rapidly decreasing (blue bar in Fig. 3) resulting in an increase in $\Delta^{13}C$ prior to the increase in $\delta^{13}C_{carb}$, and implies a change in the isotopic fractionation between total organic carbon (TOC) and sedimentary carbonate (i.e., $\Delta^{13}C$) may have taken place during the lead up to the positive $\delta^{13}C_{carb}$ excursion. As a result, we have a potential example of both process-oriented variables (f_{org} and $\Delta^{13}C$) changing at different times and in different manners during a single event. Possible explanations for increased organic carbon burial during the excursion (increased f_{org}) have been discussed extensively in the literature (e.g., Munnecke et al., 2003; Cramer and Saltzman, 2005; Cramer and Saltzman, 2007a, 2007b; Emsbo, 2017; Smolarek et al., 2017; Young et al., 2019; Young et al., 2020). However, the apparent decoupling of the carbon isotopic record and increase in $\Delta^{13}C$ immediately prior to the onset of the Ireviken positive $\delta^{13}C_{carb}$ excursion have not been evaluated previously and potential driving mechanisms for these relationships are evaluated below.

5.2. Carbon isotope fractionation

The carbon isotopic differences between components of the ocean-atmosphere (Fig. 6) are driven by four processes that impart fractionations between various carbon pools (Hayes et al., 1999). The fractionation between dissolved CO_2 and dissolved inorganic carbon (DIC) is temperature dependent and averages ~0.12‰/°C, where fractionation is stronger in colder water. Fractionation between DIC and carbonate minerals ($CaCO_3$ in Fig. 6) is weakly temperature dependent as well as

Table 1
Decoupling $\delta^{13}C_{carb}$ and $\delta^{13}C_{org}$ at the onset of the Ireviken Carbon Isotope Excursion: $\Delta^{13}C$ and organic carbon burial (f_{org}) during a Silurian oceanic anoxic event.

	$\delta^{13}C_{carb}$	$\delta^{13}C_{incoming}$	f_{org}	$\Delta^{13}C_{(carb\text{-}org)}$
Prior to excursion	+1.5‰	−5‰	0.22	+29.5‰
During excursion	+5.0‰	−5‰	0.31	+32.0‰
Excursion onset	+2.5‰	−5‰	0.24	+31.5‰

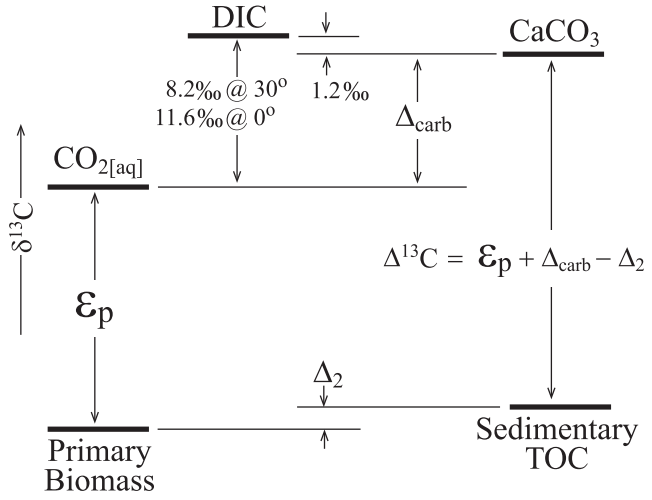

Fig. 6. Schematic diagram showing the isotopic differences between various pools of carbon in the ocean (Hayes et al., 1999). Carbon isotope values increase towards the top of the diagram. DIC = Dissolved Inorganic Carbon. $CaCO_3$ = carbonate minerals sampled for $\delta^{13}C_{carb}$. TOC = Total Organic Carbon. ε_p = fractionation efficiency of photosynthetic fixation of CO_2, $\Delta^{13}C$ = isotopic difference between sedimentary total organic carbon and carbonate minerals, Δ_{carb} = total isotopic difference between $CO_{2[aq]}$ and carbonate minerals ($CaCO_3$), and Δ_2 = total isotopic difference between original primary biomass and sedimentary total organic carbon.

weakly dependent on $[CO_3^{2-}]$ (Spero et al., 1997; Hayes et al., 1999). However, this value is typically small and a difference of 1.2‰ (Hayes et al., 1999) is used to arrive at the total isotopic difference (Δ_{carb}) between $CO_{2(aq)}$ and $CaCO_3$ of +7.0‰ at 30 °C (8.2–1.2‰) and 10.4‰ at 0 °C (11.6–1.2‰).

The creation of organic carbon molecules by photoautotrophs includes a large fractionation during fixation of CO_2 and the production of primary biomass (e.g., Falkowski, 2003). The total isotopic difference, or fractionation efficiency (ε_p), is strongly negative and can be up to −25‰, however it appears that at least for modern marine phytoplankton that photosynthetic fractionation efficiency does not exceed −25‰ (Hayes et al., 1999; Falkowski, 2003). Of course we do not typically measure the carbon isotopic value of primary biomass from the Paleozoic rock record and instead we measure the $\delta^{13}C_{org}$ of sedimentary total organic carbon (TOC). The whole range of possible fractionations between original primary biomass and sedimentary TOC (e.g., diagenesis, distillation, thermal maturation, degradation, admixture of chemoautotrophic carbon, etc.) are summarized as the term Δ_2 (Fig. 6) and can be the result of both biotic and abiotic processes. Oxidative recycling of organic carbon will leave the remaining sedimentary TOC enriched in ^{13}C compared to original primary biomass and as a result the term is often given an average value of +1.2‰ under 'normal' oxidative conditions (Hayes et al., 1989; Fischer et al., 1998; Hayes et al., 1999). The total measured isotopic difference ($\Delta^{13}C$) between carbonate minerals ($CaCO_3$) and sedimentary TOC is therefore the sum of these processes (Eq. (2), Fig. 6). As a result, the increase in $\Delta^{13}C$ prior to the onset of the ICIE should be driven by one of these three factors (ε_p, Δ_{carb}, or Δ_2) and a discussion of each parameter is included below.

$$\Delta^{13}C = \varepsilon_p + \Delta_{carb} - \Delta_2 \quad (2)$$

5.3. Fractionation of carbonate carbon (Δ_{carb})

Δ_{carb} is strongly temperature dependent and weakly dependent on $[CO_3^{2-}]$ (Spero et al., 1997; Hayes et al., 1999). At a rate of ~0.12‰/°C, a change of +2.0‰ in $\Delta^{13}C$ during the onset of the IEE (29.5‰ to 31.5‰, blue box in Fig. 3) would require a temperature change of −16.67 °C if the changes in Δ_{carb}, and consequently $\Delta^{13}C$ were driven by temperature alone. Not only is this an exceptionally large and unlikely temperature change for a tropical setting such as Gotland during the Silurian (Fig. 1), what evidence there is of temperature change related to the IBE place the onset of temperature change significantly after the onset of the positive $\delta^{13}C_{carb}$ excursion (e.g., Lehnert et al., 2010; Trotter et al., 2016, but also see Cummins et al., 2014). Given that the dependence of Δ_{carb} on $[CO_3^{2-}]$ is even smaller than temperature, and would have been starting from a likely higher initial value of Silurian pCO_2 than present atmospheric levels (e.g., Berner, 2006; Schachat et al., 2018), which would have had a diminishing effect on the role of $[CO_3^{2-}]$, it seems unlikely that any control on Δ_{carb} could have been large enough to make changes in Δ_{carb} primarily responsible for the +2.0‰ change in $\Delta^{13}C$.

5.4. Primary biomass fractionation efficiency (ε_p)

Changes in the fractionation efficiency of photosynthesis (ε_p) are most often invoked as the driver of changes in $\Delta^{13}C$ due to the impact of CO_2 concentration on ε_p (e.g., Bidigare et al., 1997; Popp et al., 1998; Kump and Arthur, 1999). However, multiple factors control ε_p (Eq. (3)) including volume to surface area ratio of the measured photosynthetic cell (V/S) and the cellular growth rate (μ), in addition to CO_2 concentrations. Eq. (3) can be rewritten to solve for CO_2, measured here in μmol/kg, to provide Eq. (4).

$$\varepsilon_p = 25.3\text{–}182\left(\mu \Big/ [CO_2]_{aq}\right)(V/S) \quad (3)$$

$$[CO_2]_{aq} = 182\,\mu(V/S) \Big/ \left(25.3 - \varepsilon_p\right) \quad (4)$$

Given the fact that we will likely never be able to measure changes in the volume to surface area ratio of primary marine organic matter directly from Paleozoic sediments, we follow Hayes et al. (1999) and hold V/S = 1 for all diagrams and calculations presented here. Given that caveat, the relationship between CO_2, growth rate, and ε_p is shown in Fig. 7. This relationship is nearly identical to the relationship between $[CO_2]_{aq}$, $[PO_4]$, and ε_p (e.g., Rau et al., 1997; Bidigare et al., 1997; Kump and Arthur, 1999; Pagani et al., 1999), illustrating that growth rate is typically a function of nutrient availability (Fig. 7). To investigate potential controls of either growth rate (μ), $[PO_4]$, or CO_2, on ε_p, we take the $\Delta^{13}C$ values from our data, subtract 7.0‰ (Δ_{carb} at 30 °C) and temporarily hold Δ_2 constant at 0.0‰ to evaluate what would be required to produce the necessary changes in ε_p if one of these three parameters was solely responsible for the +2.0‰ change in $\Delta^{13}C$ during the IEE (blue box in Fig. 3, 22.5‰ to 24.5‰ in Fig. 7, compare Table 1).

5.4.1. CO_2

The initial point in Fig. 7 is placed at a position of 22.5‰ for ε_p (calculated from our data) and given a starting CO_2 value of 32.5 μmol/kg. This initial CO_2 value is slightly more than three times the pre-industrial atmospheric CO_2 levels (Ciais et al., 2013) and is likely a conservative CO_2 estimate for the Silurian (Berner, 2006; Schachat et al., 2018). The objective of this exercise, however, is not to calculate precise total values of change, but rather to evaluate the scale of changes and their sense of direction (increasing or decreasing) that would be required to produce the data presented herein. Of course any change in the initial chosen CO_2 values will impact the position of the points shown in Fig. 7, however, the general scales and sense of directions required will not change.

Two scenarios are shown in Fig. 7. The first, arrow A, is a demonstration of the change in CO_2 required if growth rate (or $[PO_4]$) were held constant and CO_2 was the only driver responsible for the change in ε_p. In this scenario, CO_2 would have to increase by ~109 μmol/kg, which is greater than 3000 ppmv! Not only is this an exceptional, albeit not impossibly rapid increase, all available sedimentological and geochemical proxy evidence argue against such a hyperthermal in this interval of the Silurian. As discussed above, available temperature proxy

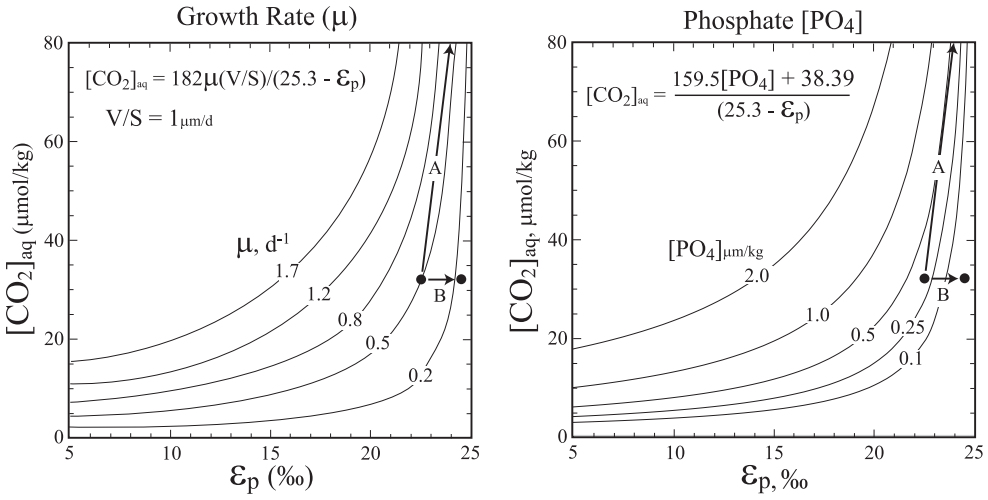

Fig. 7. A) Diagram derived from Eqs. (3) and (4) in the text (Hayes et al., 1999). Arrow A demonstrates the magnitude of change required from $[CO_2]_{aq}$ if it were the only factor changing ε_p and if we assume growth rate was constant. Arrow B demonstrates the reduction in growth rate required if it were the only factor changing ε_p and if we assume $[CO_2]_{aq}$ was constant. B) Diagram derived from Pagani et al. (1999) and Kump and Arthur (1999). Notice the overall similarities between Panels A and B illustrating the primary control of $[PO_4]$ on growth rate. Arrow A shows $[CO_2]_{aq}$ change required as in Panel A. Arrow B illustrates the reduction in $[PO_4]$ required if it were the only factor changing ε_p and if we assume $[CO_2]_{aq}$ was constant. Here we used 25.3‰ instead of 25‰ (see Kump and Arthur, 1999) for the maximum enzymatic isotope effect to follow Hayes et al. (1999) and make identical assumptions for both panels. Kump and Arthur (1999) assumed an 8‰ difference between $\Delta^{13}C$ and ε_p instead of the 7‰ difference used in Hayes et al. (1999) and utilized here.

($\delta^{18}O$) data do not record any such increase in this interval (Bickert et al., 1997; Munnecke et al., 2003; Lehnert et al., 2010; Cummins et al., 2014; Trotter et al., 2016). Furthermore, the Upper Visby Formation records a progressive shallowing upwards succession before the eventual transgression near the base of the Högklint Formation (Samtleben et al., 1996; Munnecke et al., 2003; Cramer and Saltzman, 2005, 2007b; Cramer et al., 2010). Finally, the most obvious way to produce such an increase in CO_2 would be in a Paleocene-Eocene Thermal Maximum (PETM)-like scenario with the potential release of large amounts of carbon in the form of methane (or some other similarly ^{13}C-depleted pool of carbon) resulting in rapid global warming (e.g., Panchuk et al., 2008; Meissner et al., 2014; Gehler et al., 2016; Penman and Zachos, 2018). The major difficulty with such a scenario here is that there is no attendant decrease in $\delta^{13}C_{carb}$, which is the hallmark of the PETM, and required for similar scenarios.

The combined temperature proxy data, sedimentological evidence for falling global sea level, and lack of ^{13}C-depleted signal in the $\delta^{13}C_{carb}$ record all argue against a significant increase in CO_2 as the primary driver for changes in ε_p to have been the cause of the +2.0‰ increase in $\Delta^{13}C$ at the onset of the IBE (blue box in Fig. 3). However, the available evidence (particularly the temperature proxy data) cannot rule out an extremely short-lived, extremely large, increase in CO_2 as a potentially significant influence on ε_p during the onset of the IBE (blue box in Fig. 3, see Section 5.6 below).

5.4.2. Growth rate (μ)

The second scenario for changing ε_p is to vary growth rate (μ in Eqs. (3) and (4)) by either changing the dominant organism contributing carbon to the sedimentary TOC pool (e.g., Pancost et al., 1999), or more typically, by changing the nutrient availability of the water column (Rau et al., 1997; Bidigare et al., 1997; Kump and Arthur, 1999; Pagani et al., 1999). The position of the initial point in Fig. 7 comes from the intersection of a value of 22.5‰ for ε_p (calculated from our data) and an initial CO_2 value of 32.5 μmol/kg (as with our discussion above). The resulting values of 0.5 for μ, and 0.33mMol for $[PO_4]$ (Fig. 7), are both typical of generally oligotrophic environments (Bidigare et al., 1997; Pagani et al., 1999). A total change of +2.0‰ in ε_p driven exclusively by changes in growth rate (and/or $[PO_4]$), would require a greater than 70% reduction in growth rate (or nutrient availability) and suggest hyper-oligotrophic conditions (Fig. 7).

Oligotrophy during the main body of the positive $\delta^{13}C_{carb}$ excursion (e.g., Högklint and Tofta formations, during the ICIE) has been widely discussed in the literature (e.g., Jeppsson et al., 1995; Samtleben et al., 1996; Bickert et al., 1997; Brunton et al., 1998; Munnecke et al., 2003; Cramer and Saltzman, 2005, 2007b). However, for the interval at the onset of the IEE (prior to the ICIE), the available sedimentological evidence from Gotland, and elsewhere globally, suggest a potentially significant increase in major and trace element concentrations in the interval leading up to the onset of the ICIE (blue box in Fig. 3, Jeppsson, 1997; Munnecke et al., 2003; Cramer et al., 2006; McLaughlin et al., 2012; Vandenbroucke et al., 2015; Emsbo et al., 2015, Emsbo, 2017; Smolarek et al., 2017; McAdams et al., 2019; Young et al., 2019; Richardson et al., 2019), not a scenario for reduced nutrient availability and reduced growth rates. Whereas the references provided above do not include direct proxies for primary productivity or overall nutrient availability, many provide evidence for and/or discussion of extreme abundance of both Fe and Mn in the sedimentary record of widely separated sections across multiple paleocontinents and within multiple basins at the exact same chronostratigraphic position as the blue box in Fig. 3 (i.e., immediately prior to the onset of the ICIE), which also co-occurs with the expansion of reducing environments in the marine realm (Young et al., 2019).

The significance of enhanced Fe and Mn abundance in strata deposited during the onset of the IBE (blue box in Fig. 3) is twofold. First, Fe is an integral component of oceanic biogeochemistry and is often considered a bio-limiting nutrient to phytoplankton in many areas of the modern ocean (e.g., Schoffman et al., 2016; Tagliabue et al., 2017), and Mn plays a critical role as a micronutrient in photosystem II (Raven et al., 1999; Nelson and Junge, 2015). Secondly, as discussed in Emsbo (2017), and supported by the data presented in Young et al. (2019), an expansion of reducing environments and/or euxinia at the onset of the IBE would have had the effect of remobilizing Fe and Mn that had previously been bound as FeMn-oxides in crusts and nodules on the sea floor. That would be significant not only for the release of Fe and Mn into the water column, but also the concomitant potential release of PO_4 (Lenton and Watson, 2000; Paytan and McLaughlin, 2007), which is often bound to FeMn-oxides in oxygenated settings (Fe-P burial feedback in Saltzman, 2005). Therefore, the abundance of Fe and Mn in sediments contemporaneous with the decoupled $\delta^{13}C_{carb}$ and $\delta^{13}C_{org}$ records immediately prior to the onset of the ICIE (blue box in Fig. 3) suggests the potential for enhanced nutrient availability, not a significant drop in nutrient availability. However, it is important to note that

most of the available major and trace element data that span the IEE only report total ppm of Fe and Mn, and do not provide a complete suite of elemental data or include discriminations to normalize for detrital input. Without such data it remains unclear if the sedimentary abundances are primary the result of detrital input, the particulate shuttle, recycling and enrichment within the sediment column, changes in redox state at or near the sediment-water interface, or truly represent enhanced availability of those elements in the overlying water column (e.g., Algeo and Tribovillard, 2009; Little et al., 2015).

Paleontological proxy evidence available for primary productivity during this interval from Gotland (acritarchs/g sediment, see Servais et al., 2008 for discussion of acritarchs as phytoplankton) does suggest a significant (nearly 10×) increase coincident with the negative excursion in $\delta^{13}C_{org}$ (blue box in Fig. 3; Gelsthorpe, 2002, 2004; Vandenbroucke et al., 2013). This was also coincident with an increasing difference between bulk $\delta^{13}C_{org}$ values of the sediment, organic carbon isotopic values of chitonozoans ($\delta^{13}C_{chit}$), and organic carbon isotope values of scolecodonts ($\delta^{13}C_{scol}$) where the scolecodonts had the most negative values during this negative excursion (Vandenbroucke et al., 2013). Those authors explained the ^{12}C-enriched $\delta^{13}C_{org}$ values in scolecodonts during this interval as potentially being a result of the scolecodont infaunal/benthic habitat, their increasing consumption of primary products in this interval (as opposed to partially remineralized organic carbon), and the possibility of incorporation of bacterially respired CO_2 from within the sediment (see Section 5.5 below) during the IEE.

Therefore, given the lack of sedimentological evidence for enhanced oligotrophy immediately prior to the onset of the positive $\delta^{13}C_{carb}$ excursion (blue box in Fig. 3), the potential evidence for the addition of biologically significant nutrients such as Fe and Mn (and potentially PO_4, Lenton and Watson, 2000; Paytan and McLaughlin, 2007; Young et al., 2019) to the oceans in this interval, and the paleontological proxy evidence of enhanced productivity at this level on Gotland (Gelsthorpe, 2002, 2004; Vandenbroucke et al., 2013), it is difficult to consider a reduction in growth rate (or nutrient availability, Fig. 7) as a potential primary cause of the +2.0‰ increase in $\Delta^{13}C$ via increased ε_p during the interval immediately prior to the onset of the ICIE (blue box in Fig. 3). The net result of the discussion here, and above in Section 5.4.1, is that neither changes in CO_2 nor growth rate (nor nutrient availability) appear to be likely candidates to have changed ε_p in such a way as to force a +2.0‰ change in $\Delta^{13}C$ during the onset of the IBE (blue box in Fig. 3). Therefore, the only parameter left to investigate from Eq. (2) is Δ_2, the difference between original photosynthetic primary biomass and sedimentary TOC.

5.5. Secondary sedimentary organic processes (Δ_2)

The most obvious and common sedimentary organic process that produces differences between the carbon isotopic values of primary biomass and sedimentary TOC is oxidative respiration of organic carbon either within the water column, at the sediment-water interface, or within the sediment column itself. Typical respiratory remineralization under oxygenated conditions enrich the remaining TOC in ^{13}C by preferentially recycling ^{12}C back into the water column (see discussion in Hayes et al., 1999). Whereas the value of Δ_2 imparted by respiratory remineralization of organic carbon can range from 0‰ up to +3‰ depending primarily on the percentage of primary biomass recycled (Hayes et al., 1999; Laarkamp and Raymo, 1995; Gong and Hollander, 1997; Fischer et al., 1998), none of these values are negative and therefore cannot be considered as possible drivers of our $\Delta^{13}C$ signal.

Negative Δ_2 values occur when secondary inputs of chemoautotrophic organic carbon are added to sedimentary TOC because chemoautotrophic organisms typically fix CO_2 (or CH_4) well below the photic zone where the DIC pool is enriched in ^{12}C compared to the surface ocean. Examples of significant lowering of $\delta^{13}C_{org}$ values compared to primary biomass due to the addition of chemoautotrophic organic carbon have been demonstrated from the Black Sea (e.g., Karl and Knauer, 1991; Arthur et al., 1994; Kodina et al., 1996). The seminal work of Gong and Hollander (1997) also showed a similar effect of chemoautotrophic contribution to the $\delta^{13}C_{org}$ values of sedimentary TOC from the Santa Monica Basin. The data presented here (Fig. 3), which show a rapid transient decrease in $\delta^{13}C_{org}$ decoupled from slightly rising $\delta^{13}C_{carb}$ values (Figs. 3 and 8), can be best explained by the addition of organic carbon from chemoautotrophic sources during the onset of the IBE (Fig. 8).

Biomarker and compound specific carbon isotope analysis of preserved organic matter would, of course, be the best way to demonstrate the addition of chemoautotrophic carbon to the sedimentary TOC of the Altajme Core during the onset of the IBE. Unfortunately that was beyond the initial scope of this study, but is an obvious next step in this investigation. Thankfully, a handful of samples ($n = 8$) were processed from Gotland for lipid biomarker analysis through the IEE by Rohrssen (2013). The biomarker data from Gotland illustrate major contributions of chemoautotrophic organic carbon to sedimentary TOC during the IEE, with a significant input of organic matter likely derived from methanotrophic bacteria (3β-methylhopanes, 3-MeHI >16%) and an additional contribution of 2α-methylhopanes, likely from marine cyanobacteria. Hopane/sterane (H/S) ratios are also above the Phanerozoic average (0.5–2.0, Cao et al., 2009) during the negative excursion in $\delta^{13}C_{org}$ prior to the onset of the ICIE (blue box in Fig. 3). H/S values as high as 3.8 during this interval (Rohrssen, 2013) further suggest an elevated contribution of bacterial carbon to sedimentary TOC.

These data, although limited in their number and stratigraphic coverage, provide compelling support for the addition of chemoautotrophic organic carbon to sedimentary TOC as the likely cause of the negative excursion in $\delta^{13}C_{org}$ and the initial increase in $\Delta^{13}C$ during the IEE and prior to the onset of the ICIE we recovered from the Altajme Core. It is also interesting to note that marine Anaerobic Oxidation of Methane (AOM) can utilize either sulfate as the terminal electron acceptor, or, can utilize metal oxides, specifically Fe and Mn (Beal et al., 2009; Scheller et al., 2016). The temporal relationship between Fe- and Mn-rich strata on Gotland (Emsbo, 2017) and the extremely high 3-MeH Indices (Rohrssen, 2013) may suggest a causal relationship between these two features of the sedimentary record of the IEE and further study is certainly warranted. Regardless of this potential relationship however, there is clear evidence of enhanced chemoautotrophic activity and/or preservation during the IEE coincident with the initiation of decoupled $\delta^{13}C_{carb}$ and $\delta^{13}C_{org}$ records on Gotland.

5.6. The Ireviken oceanic anoxic event

The paired carbon isotope data presented here, combined with recently published major and trace element (Emsbo, 2017; Smolarek et al., 2017) and sulfur isotope data (Rose et al., 2019; Richardson et al., 2019; Young et al., 2019, 2020), begin to demonstrate a cascade of events during the IBE that are strikingly similar to Cretaceous Oceanic Anoxic Events (OAEs), and specifically the events surrounding the Cenomanian-Turonian Boundary OAE2 (e.g., Sinton and Duncon, 1997; Kerr, 1998; Snow et al., 2005; Mort et al., 2007; Turgeon and Creaser, 2008; Hetzel et al., 2009; Adams et al., 2010; Barclay et al., 2010; Owens et al., 2013; Du Vivier et al., 2015; Ostrander et al., 2017; Eldrett et al., 2017; Jenkyns et al., 2017; Clarkson et al., 2018; Raven et al., 2018). Whereas a variety of causative links and mechanisms have been proposed in the literature, there is growing consensus that the initiation of Large Igneous Province (LIP) volcanism played a pivotal role in the initiation of OAE2 (Adams et al., 2010; Barclay et al., 2010; Du Vivier et al., 2015). Some of these models focus on the role of CO_2 and the consequent effects elevated CO_2 would have on silicate weathering, and ultimately, nutrient delivery to the oceans (e.g., Jenkyns et al., 2017; Clarkson et al., 2018). Others have focused more on the potential effects LIP volcanism would have on developing hydrothermal systems capable of delivering volumetrically significant metal-rich plumes of biologically important major and trace elements to the oceans that both stimulated

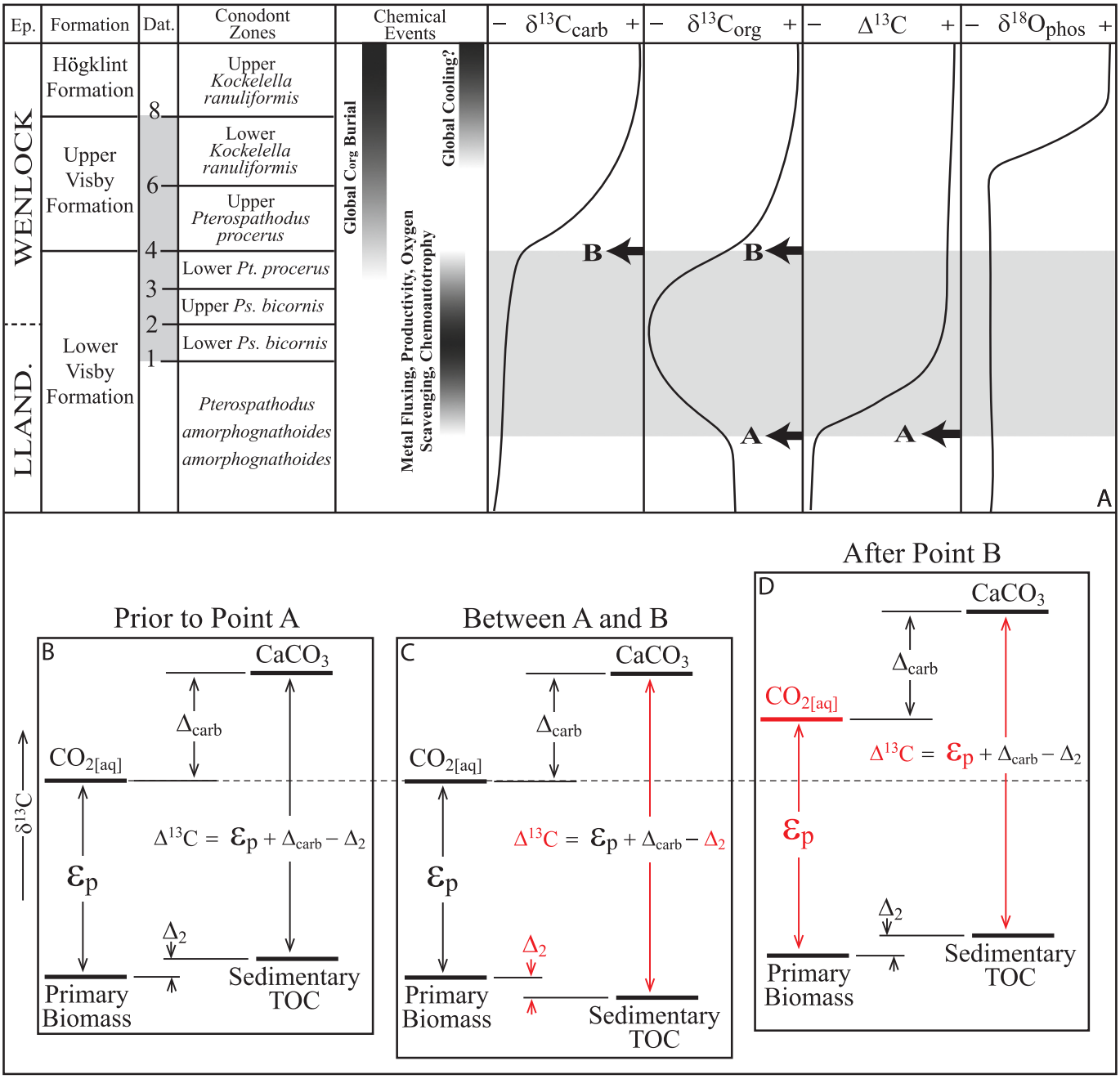

Fig. 8. A) Diagram comparing generalized trends in $\delta^{13}C_{carb}$, $\delta^{13}C_{org}$, $\Delta^{13}C$, and $\delta^{18}O_{phos}$ with major chemical events through the onset of the Ireviken Biogeochemical Event (IBE). Ep. = Epoch. Column labelled "Dat." refers to extinction datum levels of the Ireviken Extinction Event (IEE) (Jeppsson, 1987, 1997) and the grey box in this column illustrates the duration of the IEE. Datum points 1–8 of the IEE defined by Jeppsson, 1987, 1997 include: 1) Last Appearance Datum (LAD) of *Nudibelodina sensitiva*, 2) LADs of *Ozarkodina polinclinata polinclinata*, *Apsidognathus ruginosus* and *Apsidognathus walmsleyi*, 3) LAD of *Pterospathodus amorphognathoides amorphognathoides*, 4) First Appearance Datum (FAD) of *Ozarkodina paraconfluens* and temporary disappearance of *Panderodus panderi*, 6) LAD of *Pterospathodus pennatus procerus*, 8) LAD of *Distomodus staurognathoides* and FAD of *Ozarkodina martinssoni*. Global cooling is shown with a question mark due to the fact that $\delta^{18}O_{carb}$ (e.g., Munnecke et al., 2003) and $\delta^{18}O_{phos}$ (e.g., Lehnert et al., 2010) data show a positive excursion beginning at different times, and isotopologue data (Cummins et al., 2014) shows little to no variation in the interval altogether. This issue warrants considerable further high-resolution study. Point A (Arrow at bottom of grey box in Panel A) illustrates the onset of the geochemical event, either through potential LIP initiation or SEDEX brine expulsion, or some other unrecognized cause. Point B illustrates the onset of the positive carbonate carbon excursion responding to the increase in organic carbon burial (f_{org}). B-D) diagrams showing which parameters likely changed during each point in the top diagram. The shaded box denotes the onset of the IBE, equivalent to the blue box in Fig. 3. B) Prior to point A, the standard diagram (Fig. 5). C) From point A to point B, metal fluxing, oxygen scavenging, and increased productivity lead to chemoautotrophy generating a drop in Δ_2, which produced a drop in $\delta^{13}C_{org}$ and the initial positive increase in $\Delta^{13}C$. D) After point B, the $\delta^{13}C_{carb}$ increases due to increased global C_{org} burial (f_{org} increase). (For interpretation of the references to colour in this figure legend, the reader is referred to the web version of this article.)

productivity as well as had the potential to reach toxic levels (e.g., Snow et al., 2005). In this scenario, the delivery of major and trace metals to the oceans were the ultimate driver of anoxia, via enhanced productivity, as well as a major driver of biotic turnover through elevated toxicity.

The Ireviken Biogeochemical Event (IBE) has been proposed to have been triggered by a similar mass introduction of redox-sensitive major and trace elements into the ocean as well (Emsbo, 2017), however, in that author's case not from LIP volcanism but from Sedimentary Exhalative (SEDEX) ore brine expulsion. The scenario is virtually identical, in that mass introduction of redox sensitive elements to the ocean have a two-fold consequence: 1) the introduction of toxic levels of elements into the ocean leading to an initial phase of biocrisis and teratology (e.g., Vandenbroucke et al., 2015), and 2) the concomitant drawdown of available oxygen in the oceans due to scavenging by reduced metals and the simultaneous increase in primary productivity driving oxygen demand. The net result would be expanded anoxia/euxinia that leads to increase organic carbon burial and the positive carbonate carbon isotope excursion (e.g., Cramer and Saltzman, 2005; Cramer et al., 2006; Cramer and Saltzman, 2007b). Importantly, this potential expansion of euxina was recently supported by $\delta^{34}S$ data as well (Young et al., 2019; Rose et al., 2019; Richardson et al., 2019). This series of events, particularly the demonstration of in-vivo uptake of toxic trace metals coincident with teratology during the IEE (Vandenbroucke et al., 2015), make the scenario described by Snow et al. (2005) an attractive comparison between OAE2 and the Ireviken Biogeochemical Event.

Whereas the scenario presented by Emsbo (2017) fits well with the discussion above, it is important to note that the identification of a specific deposit (Howard's Pass) as the trigger for the IBE is not supported by the biostratigraphic data available. Both conodont and graptolite biostratigraphy available from Howard's Pass (e.g., Norford and Orchard, 1985) demonstrate that the interval of mineral emplacement was no higher than the lowest Telychian, and was more likely limited to a position within the Rhuddanian to Aeronian stages of the Llandovery (*cyphus* to *convolutus* graptolite Zones, *kentuckyensis* conodont Zone). This is many millions of years prior to the IBE and, therefore, the event that led to the emplacement of the Howard's Pass deposit is unlikely to have been responsible for the IBE. However, the general scenario presented remains valid, even if the identification of a specific deposit as the cause is not supported by biostratigraphy.

A scenario of either SEDEX or LIP emplacement could easily produce the paired data presented herein (Fig. 8), where the introduction of redox-sensitive major and trace elements to the oceans drives an initial interval of chemoautotrophy leading to lowering of Δ_2 during the onset of the IEE (Fig. 8 panel C). It could also be that a short-lived massive increase in CO_2 due to initiation of a LIP played a role in this interval as well, however, the limited $\delta^{18}O_{[PO4]}$ data available and sequence stratigraphy of this interval do not appear to support this hypothesis. Then, as oxygen scavenging and enhanced oxygen demand from primary productivity lowers the oxygen content of bottom waters available to recycle organic carbon, increased organic carbon burial begins to take over (the Ireviken OAE) leading to enhanced organic carbon preservation, an increase in f_{org}, and the ICIE. During this interval (after point B in Fig. 8), the isotopic value of $CO_{2[aq]}$ increases due to enhanced organic carbon burial, but $\Delta^{13}C$ remains elevated and, in fact, increases even more. This could either be due to enhanced oligotrophy (essentially arrow B in Fig. 7), which is supported by the tendency towards clean carbonate reefs during this interval (Brunton et al., 1998; Cramer and Saltzman, 2007b; Calner, 2008; Cramer et al., 2010), or it could be that Δ_2 remains lower than pre-event values due to the sustained presence of chemoautotrophs such as bacterial sulfate reducers (e.g., Young et al., 2019) or other chemoautotrophic additions to sedimentary TOC. In either case, the elevated $\delta^{13}C_{carb}$ remains a likely indicator of expanded areas of anoxic/euxinic bottom water conditions during the Ireviken OAE and this appears to be supported by the sulfur isotopic record of this interval as well that illustrates an expansion of reducing environments throughout the ICIE.

6. Conclusions

The high-resolution carbon isotope data produced by this investigation demonstrate a negative excursion in $\delta^{13}C_{org}$ and positive increase in $\Delta^{13}C$ prior to the onset of the positive $\delta^{13}C_{carb}$ excursion. The integration of these new data with pre-existing studies of the biological events surrounding the IEE demonstrate the importance of High-Resolution Integrated Stratigraphy (HiRES, Cramer et al., 2015) for investigating global biogeochemical events in the deep past. The new data presented here, together with the prior geochemical and paleontological evidence of a large influx of biologically significant elements into the ocean immediately prior to the onset of the IBE and subsequent anoxia/euxinia (Gelsthorpe, 2002; Rohrssen, 2013; Vandenbroucke et al., 2013, 2015; Emsbo, 2017; Smolarek et al., 2017; Young et al., 2019, 2020) set up a scenario for the cascade of events that produced the Ireviken OAE.

Similar to OAE2 across the Cenomanian-Turonian boundary in the Cretaceous, the introduction of these biologically significant elements into the ocean during the late Llandovery would have scavenged available oxygen largely through initially enhanced primary productivity, generating an expansion of oceanic anoxia/euxinia, and promoting the addition of chemoautotrophic organic carbon into the sedimentary TOC record. The expansion of anoxic/euxinic conditions (e.g., Young et al., 2019) generated an increase in organic carbon burial (increased f_{org}), which ultimately led to the positive $\delta^{13}C_{carb}$ excursion that has been documented worldwide. During this Silurian example, the initiation of the event has been proposed to be the expulsion of a SEDEX ore brine (Emsbo, 2017), whereas during the OAE2 it appears to have been the emplacement of Large Igneous Province (LIP, Snow et al., 2005; Adams et al., 2010; Barclay et al., 2010, Du Vivier et al., 2015). In both cases, the introduction of biologically significant elements in abundance into the oceans was ultimately responsible for the increase in organic carbon burial and the positive carbon isotope excursion. Whether or not the Ireviken Biogeochemical Event was the result of a SEDEX expulsion event or a Large Igneous Province has yet to be tested, however, it appears to preserve many of the same biogeochemical signals recorded during OAE2.

The insights into the global carbon cycle perturbations during the IBE provided by this study were the result of the extremely high-resolution isotopic sampling. The ocean-atmosphere-biosphere system operates on extremely short timescales (typically <10,000 yrs) and data resolution on similar timescales is required if we are to evaluate fully how these systems operated in the past. This work illustrates both the importance and potential of high-resolution chemostratigraphy for Paleozoic biogeochemical events and demonstrates the practicability of such studies. It is likely that a new generation of high-resolution chemostratigraphy will be required to re-evaluate most, if not all, of the major Paleozoic biogeochemical events in an effort to evaluate potential cause-and-effect mechanisms that may have been responsible for each event.

Declaration of Competing Interest

None.

Acknowledgements

This work was partially supported by National Science Foundation grant CAREER-1455030 to BDC, NASA Iowa Space Grant Consortium under Award No. NNX16AL88H to ERH, and Natural Sciences and Engineering Research Council of Canada Discovery Grant to MJM. We thank Alexa Hanson and Nick Lefler who helped to drill the carbonate carbon isotope samples from the core. This research was completed as an honors undergraduate senior thesis project (E.R. Hartke) at the

University of Iowa, Department of Earth and Environmental Sciences.

Appendix A. Supplementary data

Supplementary data to this article can be found online at https://doi.org/10.1016/j.gloplacha.2020.103373.

References

Adams, D.D., Hurtgen, M.T., Sageman, B.B., 2010. Volcanic triggering of a biogeochemical cascade during Oceanic Anoxic Event 2. Nat. Geosci. 3, 201–204. https://doi.org/10.1038/ngeo743.

Algeo, T.J., Tribovillard, N., 2009. Environmental analysis of paleoceanographic systems based on molybdenum-uranium covariation. Chem. Geol. 268, 211–225. https://doi.org/10.1016/j.chemgeo.2009.09.001.

Arthur, M.A., Dean, W.E., Neff, E.D., Hay, B.J., King, J., Jones, G., 1994. Varve-calibrated records of carbonate and organic carbon accumulation over the last 2000 years in the Black Sea. Glob. Biogeochem. Cyc. 8, 195–217. https://doi.org/10.1029/94GB00297.

Bachan, A., Lau, K.V., Saltzman, M.R., Thomas, E.T., Kump, L.R., Payne, J.L., 2017. A model for the decrease in amplitude of carbon isotope excursions across the Phanerozoic. Am. J. Sci. 317, 641–676. https://doi.org/10.2475/06.2017.01.

Bancroft, A.M., Cramer, B.D., 2020. Silurian conodont biostratigraphy of the east-central Appalachian Basin (eastern USA): re-examination of the C.T. Helfrich Collection. Bull. Geosci. 95, 1–22. https://doi.org/10.3140/bull.geosci.1748.

Barclay, R.S., McElwain, J.C., Sageman, B.B., 2010. Carbon sequestration activated by a volcanic CO_2 pulse during Oceanic Anoxic Event 2. Nat. Geosci. 3, 205–208. https://doi.org/10.1038/ngeo757.

Batchelor, R.A., Jeppsson, L., 1994. Late Llandovery bentonites from Gotland, Sweden, as chronostratigraphic markers. J. Geol. Soc. London 151, 741–746.

Beal, E.J., House, C.H., Orphan, V.J., 2009. Manganese- and iron-dependent marine methane oxidation. Science 325, 184–187. https://doi.org/10.1126/science.1169984.

Berner, R.A., 1990. Atmospheric carbon dioxide levels over Phanerozoic time. Science 249, 1382–1386. https://doi.org/10.1126/science.249.4975.1382.

Berner, R.A., 2006. GEOCARBSULF: A combined model for Phanerozoic atmospheric O_2 and CO_2. Geochim. Cosmochim. Acta 70 (23), 5653–5664. https://doi.org/10.1016/j.gca.005.11.032.

Bickert, T., Pätzold, J., Samtleben, C., Munnecke, A., 1997. Paleoenvironmental changes in the Silurian indicated by stable isotopes in brachiopod shells from Gotland, Sweden. Geochim. Cosmochim. Acta 61 (13), 2717–2730. https://doi.org/10.1016/S0016-7037(97)00136-1.

Bidigare, R.R., Fluegge, A., Freeman, K.H., Hanson, K.L., Hayes, J.M., Hollander, D., Jasper, J.P., King, L.L., Laws, E.A., Milder, J., Millero, F.J., 1997. Consistent fractionation of ^{13}C in nature and in the laboratory: growth-rate effects in some haptophyte algae. Glob. Biogeochem. Cyc. 11 (2), 279–292. https://doi.org/10.1029/96GB03939.

Brunton, F.R., Smith, L., Dixon, O.A., Copper, P., Nestor, H., Kershaw, S., 1998. Silurian reef episodes, changing seascapes and paleobiogeography. NY State Mus. Bull. 491, 259–276.

Calner, M., 2008. Silurian global events–at the tipping point of climate change. In: Mass Extinction. Springer-Verlag, Berlin and Heidelberg, pp. 21–57.

Calner, M., Jeppsson, L., Munnecke, A., 2004. The Silurian of Gotland - Part 1: review of the stratigraphic framework, event stratigraphy, and stable carbon and oxygen isotope development. Erlanger Geol. Abh. 5, 113–131.

Cao, C., Love, G.D., Hays, L.E., Wang, W., Shen, S., Summons, R.E., 2009. Biogeochemical evidence for euxinic oceans and ecological disturbance presaging the end-Permian mass extinction event. Earth Plan. Sci. Lett. 281, 188–201. https://doi.org/10.1016/j.epsl.2009.02.012.

Ciais, P., Sabine, C., Bala, G., Bopp, L., Brovkin, V., Canadell, J., Chhabra, A., DeFries, R., Galloway, J., Heimann, M., Jones, C., Le Quéré, C., Myneni, R.B., Piao, S., Thornton, P., 2013. Carbon and other biogeochemical cycles. In: Stocker, T.F., Qin, D., Plattner, G.K., Tignor, M., Allen, S.K., Boschung, J., Midgley, P.M. (Eds.), Climate Change 2013: The Physical Science Basis. Contribution of Working Group I to the Fifth Assessment Report of the Intergovernmental Panel on Climate Change. Cambridge University Press, Cambridge, United Kingdom, pp. 465–570.

Clarkson, M.O., Stirling, C.H., Jenkyns, H.C., Dickson, A.J., Porcelli, D., Moy, C.M., Pogge von Strandmann, P.A.E., Cooke, I.R., Lenton, T.M., 2018. Uranium isotope evidence for two episodes of deoxygenation during Oceanic Anoxic Event 2. Proc. Nat. Acad. Sci. 115, 2918–2923. https://doi.org/10.1073/pnas.1715278115.

Cooper, R.A., Sadler, P.M., Munnecke, A., Crampton, J.S., 2014. Graptoloid evolutionary rates track Ordovician-Silurian global climate change. Geol. Mag. 151, 349–364. https://doi.org/10.1017/S0016756813000198.

Cramer, B.D., Jarvis, I., 2020. Chapter 11: carbon isotope stratigraphy. In: Gradstein, F. M., Ogg, J.G., Schmitz, M.D., Ogg, G.M. (Eds.), Geologic Time Scale 2020, vol. 1. Elsevier, Amsterdam, pp. 309–343. https://doi.org/10.1016/B978-0-12-824360-2.00011-5.

Cramer, B.D., Saltzman, M.R., 2005. Sequestration of ^{12}C in the deep ocean during the early Wenlock (Silurian) positive carbon isotope excursion. Palaeogeogr. Palaeoclimatol. Palaeoecol. 219 (3–4), 333–349. https://doi.org/10.1016/j.palaeo.2005.01.009.

Cramer, B.D., Saltzman, M.R., 2007a. Early Silurian paired $\delta^{13}C_{carb}$ and $\delta^{13}C_{org}$ analyses from the Midcontinent of North America: implications for paleoceanography and paleoclimate. Palaeogeogr. Palaeoclimatol. Palaeoecol. 256, 195–203. https://doi.org/10.1016/j.palaeo.2007.02.032.

Cramer, B.D., Saltzman, M.R., 2007b. Fluctuations in epeiric sea carbonate production during Silurian positive carbon isotope excursions: a review of proposed paleoceanographic models. Palaeogeogr. Palaeoclimatol. Palaeoecol. 245 (1–2), 37–45. https://doi.org/10.1016/j.palaeo.2006.02.027.

Cramer, B.D., Saltzman, M.R., Kleffner, M.A., 2006. Spatial and temporal variability in organic carbon burial during global positive carbon isotope excursions: new insight from high resolution $\delta^{13}C_{carb}$ stratigraphy from the type area of the Niagaran (Silurian) Provincial Series. Stratigraphy 2, 327–340.

Cramer, B.D., Loydell, D., Samtleben, C., Munnecke, A., Kaljo, D., Männik, P., Martma, T., Jeppsson, L., Kleffner, M., Barrick, J., Johnson, C., Emsbo, P., Joachimski, M., Bickert, T., Saltzman, M.R., 2010. Testing the limits of Paleozoic chronostratigraphic correlation via high-resolution (<500 k.y.) integrated conodont, graptolite, and carbon isotope ($\delta^{13}C_{carb}$) biochemostratigraphy across the Llandovery–Wenlock (Silurian) boundary: is a unified Phanerozoic time scale achievable? GSA Bull. 122 (9–10), 1700–1716. https://doi.org/10.1130/B26602.1.

Cramer, B.D., Brett, C.E., Melchin, M.J., Männik, P., Kleffner, M.A., McLaughlin, P.I., Loydell, D.K., Munnecke, A., Jeppsson, L., Corradini, C., Brunton, F.R., Saltzman, M. R., 2011. Revised correlation of Silurian Provincial Series of North America with global and regional chronostratigraphic units and $\delta^{13}C_{carb}$ chemostratigraphy. Lethaia 44, 185–202. https://doi.org/10.1111/j.1502-3931.2010.00234.x.

Cramer, B.D., Condon, D.J., Söderlund, U., Marshall, C., Worton, G.J., Thomas, A.T., Calner, M., Ray, D.C., Perrier, V., Boomer, I., Patchett, P.J., 2012. U-Pb (zircon) age constraints on the timing and duration of Wenlock (Silurian) paleocommunity collapse and recovery during the "Big Crisis". GSA Bull. 124 (11–12), 1841–1857. https://doi.org/10.1130/B30642.1.

Cramer, B.D., Vandenbroucke, T.R.A., Ludvigson, G.A., 2015. High-resolution event stratigraphy (HiRES) and the quantification of stratigraphic uncertainty: Silurian examples of the quest for precision in stratigraphy. Earth Sci. Rev. 141, 136–153. https://doi.org/10.1016/j.earscirev.2014.11.011.

Crampton, J.S., Cooper, R.A., Sadler, P.M., Foote, M., 2016. Greenhouse-icehouse transition in the Late Ordovician marks a step change in extinction regime in the marine plankton. Proc. Natl. Acad. Sci. 113, 1498–1503. https://doi.org/10.1073/pnas.1519092113.

Cummins, R.C., Finnegan, S., Fike, D.A., Eiler, J.M., Fischer, W.W., 2014. Carbonate clumped isotope constraints on Silurian ocean temperature and sea water $\delta^{18}O$. Geochim. Cosmochim. Acta 140, 241–258. https://doi.org/10.1016/j.gca.2014.05.024.

Danielsen, E.M., Cramer, B.D., Kleffner, M.A., 2019. Identification of a global sequence boundary within the upper Homerian (Silurian) Mulde Event: high-resolution chronostratigraphic correlation of the midcontinent United States with Sweden and the United Kingdom. Geosphere 15, 839–855. https://doi.org/10.1130/GES01685.1.

Derry, L.A., France-Lanord, C., 1996. Neogene growth of the sedimentary organic carbon reservoir. Paleoceanography 11, 267–275. https://doi.org/10.1029/95PA03839.

Du Vivier, A.D.C., Jacobson, A.D., Lehn, G.O., Selby, D., Hurtgen, M.T., Sageman, B.B., 2015. Ca isotope stratigraphy across the Cenomanian-Turonian OAE2: links between volcanism, seawater geochemistry, and the carbonate fractionation factor. Earth Planet. Sci. Lett. 416, 121–131. https://doi.org/10.1016/j.epsl.2015.02.001.

Eldrett, J.S., Dodsworth, P., Bergman, S.C., Wright, M., Minisini, D., 2017. Water-mass evolution in the Cretaceous Western Interior Seaway of North America and equatorial Atlantic. Clim. Past 13, 855–878. https://doi.org/10.5194/cp-13-855-2017.

Emsbo, P., 2017. Sedex brine expulsions to Paleozoic basins may have changed global marine $^{87}Sr/^{86}Sr$ values, triggered anoxia, and initiated mass extinctions. Ore Geol. Rev. 86, 474–486. https://doi.org/10.1016/j.oregeorev.2017.02.031.

Emsbo, P., McLaughlin, P.I., Breit, G.N., du Bray, E.A., Koenig, A.E., 2015. Rare earth elements in sedimentary phosphate deposits: solution to the global REE crisis? Gondwana Res. 27 (2), 776–785. https://doi.org/10.1016/j.gr.2014.10.008.

Falkowski, P., 2003. Biogeochemistry of primary production in the sea. Treat. Geochem. 8, 185–213. https://doi.org/10.1016/B0-08-043751-6/08129-9.

Fischer, G., Muller, P.J., Wefer, G., 1998. Latitudinal $\delta^{13}C_{org}$ variations in sinking matter and sediments from the South Atlantic: Effects of anthropogenic CO_2 and implications for palaeo-PCO_2 reconstructions. J. Mar. Sys. 17 (1–4), 471–495. https://doi.org/10.1016/S0924-7963(98)00059-1.

Frýda, J., Štorch, P., 2014. Carbon isotope chemostratigraphy of the Llandovery in northern peri-Gondwana: new data from the Barrandian area, Czech Republic. Eston. J. Earth Sci. 63 (4), 220. https://doi.org/10.3176/earth.2014.22.

Gehler, A., Gingerich, P.D., Pack, A., 2016. Temperature and atmospheric CO_2 concentration estimates through the PETM using triple oxygen isotope analysis of mammalian bioapatite. Proc. Natl. Acad. Sci. 113 (28), 7739–7744. https://doi.org/10.1073/pnas.1518116113.

Gelsthorpe, D.N., 2002. Microplankton Changes Through the Early Silurian Ireviken extinction event on Gotland, Sweden. PhD Thesis. University of Leicester, Leicester, UK.

Gelsthorpe, D.N., 2004. Microplankton changes through the early Silurain Ireviken extinction event on Gotland,Sweden. Rev. Palaeobot. and Palyno. 130, 89–103. https://doi.org/10.1016/j.revpalbo.2003.12.003.

Gong, C., Hollander, D.J., 1997. Differential contribution of bacteria to sedimentary organic matter in oxic and anoxic environments, Santa Monica Basin, California. Org. Geochem. 26, 545–563. https://doi.org/10.1016/S0146-6380(97)00018-1.

Gradstein, F.M., Ogg, J.G., Schmitz, 2020. In: Ogg, G.M. (Ed.), Geologic Time Scale 2020, 2. Elsevier, Amsterdam, pp. 809–pp.

Gruber, N., Keeling, C.D., Bacastow, R.B., Guenther, P.R., Lueker, T.J., Wahlen, M., Meijer, H.A.J., Mook, W.G., Stocker, T.F., 1999. Spatio-temporal patterns of carbon-

13 in the global surface oceans and the oceanic Suess effect. Glob. Biogeochem. Cyc. 13, 307–335. https://doi.org/10.1029/1999GB900019.
Hayes, J.M., Popp, B.M., Takigiku, R., Johnson, M.W., 1989. An isotopic study of biogeochemical relationships between carbonates and organic carbon in the Greenhorn Formation. Geochim. Cosmochim. Acta 53, 2961–2972.
Hayes, J.M., Strauss, H., Kaufman, A.J., 1999. The abundance of ^{13}C in marine organic matter and isotopic fractionation in the global biogeochemical cycle of carbon during the past 800 Ma. Chem. Geol. 161, 103–125. https://doi.org/10.1016/S0009-2541(99)00083-2.
Hetzel, A., Boettcher, M.E., Wortmann, U.G., Brumsack, H.-J., 2009. Paleo-redox conditions during OAE 2 reflected in Demerara Rise sediment geochemistry (ODP Leg 207). Palaeogeogr. Palaeoclimat. Palaeoecol. 273, 302–328. https://doi.org/10.1016/j.palaeo.2008.11.005.
Hladikova, J., Hladil, J., Kribek, B., 1997. Carbon and oxygen isotope record across Pridoli to Givetian stage boundaries in the Barrandian basin (Czech Republic). Palaeogeogr. Palaeoclimat. Palaeoecol. 132, 225–241. https://doi.org/10.1016/S0031-0182(97)00062-X.
Jenkyns, H.C., Dickson, A.J., Ruhl, M., van den Boorn, S.H.J.M., 2017. Basalt-seawater interaction, the Plenus Cold Event, enhanced weathering and geochemical change: deconstructing Oceanic Anoxic Event 2 (Cenomanian-Turonian, Late Cretaceous). Sediment 64, 16–43. https://doi.org/10.1111/sed.12305.
Jeppsson, L., 1987. Lithological and conodont distributional evidence for episodes of anomalous oceanic conditions during the Silurian. Palaeobio. Cono. 129–145.
Jeppsson, L., 1990. An oceanic model for lithological and faunal changes tested on the Silurian record. J. Geol. Soc. 147 (4), 663–674. https://doi.org/10.1144/gsjgs.147.4.0663.
Jeppsson, L., 1997. A new latest Telychian, Sheinwoodian and Early Homerian (Early Silurian) standard conodont zonation. Transact. Royal Soc. Edinburgh: Earth Sci. 88, 91–114. https://doi.org/10.1017/S0263593300006854.
Jeppsson, L., Aldridge, R.J., Dorning, K.J., 1995. Wenlock (Silurian) oceanic episodes and events. J. Geol. Soc. 152 (3), 487–498. https://doi.org/10.1144/gsjgs.152.3.0487.
Jeppsson, L., Eriksson, M.E., Calner, M., 2006. A latest Llandovery to latest Ludlow high-resolution biostratigraphy based on the Silurian of Gotland—a summary. GFF 128 (2), 109–114. https://doi.org/10.1080/11035890601282109.
Jeppsson, L., Talent, J.A., Mawson, R., Simpson, A.J., Andrew, A.S., Calner, M., Whitford, D.J., Trotter, J.A., Sandström, O., Caldon, H.J., 2007. High-resolution Late Silurian correlations between Gotland, Sweden, and the Broken River region, NE Australia: lithologies, conodonts and isotopes. Palaeogeogr. Palaeoclimatol. Palaeoecol. 245, 115–137. https://doi.org/10.1016/j.palaeo.2006.02.032.
Kaljo, D., Martma, T., Saadre, T., 2007. Post-Hunnebergian Ordovician carbon isotope trend in Baltoscandia, its environmental implications and some similarities with that of Nevada. Palaeogeogr. Palaeoclimatol. Palaeoecol. 245, 138–155. https://doi.org/10.1016/j.palaeo.2006.02.020.
Kaljo, D., Einasto, R., Martma, T., Märss, T., Nestor, V., Viira, V., 2015. A bio-chemostratigraphical test of the synchronicity of biozones in the upper Silurian of Estonia and Latvia with some implications for practical stratigraphy. Eston. J. Earth Sci. 64, 267–283. https://doi.org/10.3176/earth.2015.33.
Karl, D.M., Knauer, G.A., 1991. Microbial production and particle flux in the upper 350 m of the Black Sea. Deep-Sea Res. 38 (2), S921–S942. https://doi.org/10.1016/S0198-0149(10)80017-2.
Kerr, A.C., 1998. Oceanic plateau formation: a cause of mass extinction and black shale deposition around the Cenomanian Turonian boundary. J. Geol. Soc. 155, 619–626. https://doi.org/10.1144/gsjgs.155.4.0619.
Kiipli, T., Männik, P., Batchelor, R.A., Kiipli, E., Kallaste, T., Perens, H., 2001. Correlation of Telychian (Silurian) altered volcanic ash beds in Estonia, Sweden and Norway. Norwegian Journal of Geology 81, 179–194.
Kodina, L.A., Bogacheva, M.P., Lyutsarev, S.B., 1996. Particulate organic carbon in the Black Sea: isotopic composition and origin. Geochem. Int. 34 (9), 798–804.
Kozłowski, W., 2015. Eolian dust influx and massive whitings during the kozlowski/Lau Event: carbonate hypersaturation as a possible driver of the mid-Ludfordian Carbon Isotope Excursion. Bull. Geosci. 90 (4) https://doi.org/10.3140/bull.geosci.1581.
Kump, L.R., Arthur, M.A., 1999. Interpreting carbon-isotope excursions: carbonates and organic matter. Chem. Geol. 161, 181–198. https://doi.org/10.1016/S0009-2541(99)00086-8.
Kump, L.R., Arthur, M.A., Patzkowsky, M.E., Gibbs, M.T., Pinkus, D.S., Sheehan, P.M., 1999. A weathering hypothesis for glaciation at high atmospheric pCO_2 during the Late Ordovician. Palaeogeogr. Palaeoclimatol. Palaeoecol. 152, 173–187. https://doi.org/10.1016/S0031-0182(99)00046-2.
Laarkamp, K.L., Raymo, M.E., 1995. Carbon isotopic composition of particulate organic material from the interior of the Equatorial Pacific Ocean. In: ICP V Program and Abstracts, 5th International Conference on Paleoceanography. University of New Brunswick, Fredricton, p. 132.
Lehnert, O., Männik, P., Joachimski, M.M., Calner, M., Frýda, J., 2010. Palaeoclimate perturbations before the Sheinwoodian glaciation: a trigger for extinctions during the 'Ireviken Event'. Palaeogeogr. Palaeoclimatol. Palaeoecol. 296 (3–4), 320–331. https://doi.org/10.1016/j.palaeo.2010.01.009.
Lenton, T.M., Watson, A.J., 2000. Redfield revisited 1. Regulation of nitrate, phosphate, and oxygen in the ocean. Glob. Biogeochem. Cycl. 14 (1), 225–248. https://doi.org/10.1029/1999GB900065.
Lenz, A.C., 1982. Llandoverian Graptolites of the Northern Canadian Cordillera: Petalograptus, Cephalograptus, Rhaphidograptus, Dimorphograptus, Retiolitidae, and Monograptidae. The Alger Press, Toronto.
Little, S.H., Vance, D., Lyons, T.W., McManus, J., 2015. Controls on trace metal authigenic enrichment in reducing sediments: insights from modern oxygen-deficient settings. Am. J. Sci. 315, 77–119. https://doi.org/10.2475/02.2015.01.
Loydell, D.K., Frýda, J., 2007. Carbon isotope stratigraphy of the upper Telychian and lower Sheinwoodian (Llandovery-Wenlock, Silurian) of the Banwy River section, Wales. Geol. Mag. 144, 1015–1019. https://doi.org/10.1017/S0016756807003895.
Loydell, D.K., Sarmiento, G.N., Štorch, P., Gutiérrez-Marco, J.C., 2008. Graptolite and conodont biostratigraphy of the upper Telychian-lower Sheinwoodian (Llandovery-Wenlock) strata, Jabalon River section, Corral de Calatrava, central Spain. Geol. Mag. 146, 187–198. https://doi.org/10.1017/S0016756808005840.
Männik, P., Loydell, Nestor, V. and Nõlvak, J., 2015. Integrated Upper Ordovician-lower Silurian biostratigraphy of the Grötlingbo-1 core section, Sweden. GFF 137, 226–244. https://doi.org/10.1080/11035897.2015.1042032.
McAdams, N.E.B., Bancroft, A.M., Cramer, B.D., Witzke, B.J., 2017. Integrated carbon isotope and conodont biochemostratigraphy of the Silurian (Aeronian-Telychian) of the East-Central Iowa Basin, Iowa, USA. Newsl. Stratigr. 50, 391–416. https://doi.org/10.1127/nos/2017/0375.
McAdams, N.E.B., Cramer, B.D., Bancroft, A.M., Melchin, M.J., Devera, J.A., Day, J.E., 2019. Integrated $\delta^{13}C_{carb}$, conodont, and graptolite biochemostratigraphy of the Silurian from the Illinois Basin and stratigraphic revision of the Bainbridge Group. GSA Bull. 131, 335–352. https://doi.org/10.1130/B32033.1.
McLaughlin, P.I., Emsbo, P., Brett, C.E., 2012. Beyond black shales: the sedimentary and stable isotope records of oceanic anoxic events in a dominantly oxic basin (Silurian; Appalachian Basin, USA). Palaeogeogr. Palaeoclimatol. Palaeoecol. 367, 153–177. https://doi.org/10.1016/j.palaeo.2012.10.002.
McLaughlin, P.I., Mikulic, D.G., Kluessendorf, J., 2013. Age and correlation of Silurian rocks in Sheboygan, Wisconsin, using integrated stable carbon isotope stratigraphy and facies analysis. Geosci. Wis. 21, 15–38.
Meissner, K.J., Bralower, T.J., Alexander, K., Jones, T.D., Sijp, W., Ward, M., 2014. The Paleocene-Eocene thermal maximum: how much carbon is enough? Paleoceanography 29 (10), 946–963. https://doi.org/10.1002/2014PA002650.
Melchin, M.J., 1989. Llandovery graptolite biostratigraphy and paleobiogeography, Cape Phillips Formation, Canadian Arctic Islands. Can. J. Earth Sci. 26, 1726–1746.
Melchin, M.J., Holmden, C., 2006. Carbon isotope chemostratigraphy in Arctic Canada: Sea-level forcing of carbonate platform weathering and implications for Hirnantian global correlation. Palaeogeogr. Palaeoclimatol. Palaeoecol. 234 (2–4), 186–200. https://doi.org/10.1016/j.palaeo.2005.10.009.
Melchin, M.J., Sadler, P.M., Cramer, B.D., 2012. Chapter 21: The Silurian Period. In: Gradstein, F.M., Ogg, J.G., Schmitz, M.D., Ogg, G.M. (Eds.), The Geologic Time Scale 2020. Elsevier, Amsterdam, pp. 525–558. https://doi.org/10.1016/B978-0-444-59425-9.00021-4.
Melchin, M.J., Sadler, P.M., Cramer, B.D., 2020. Chapter 21: The Silurian Period. In: Gradstein, F.M., Ogg, J.G., Schmitz, M.D., Ogg, G.M. (Eds.), Geologic Time Scale 2020, vol. 2. Elsevier, Amsterdam, pp. 695–732. https://doi.org/10.1016/B978-0-12-824360-2.00021-8.
Mort, H.P., Adatte, T., Foellmi, K.B., Keller, G., Steinmann, P., Matera, V., Berner, Z., Stueben, D., 2007. Phosphorus and the roles of productivity and nutrient recycling during oceanic anoxic event 2. Geology (Boulder) 35, 483–486. https://doi.org/10.1130/G23475A.1.
Munnecke, A., Samtleben, C., Bickert, T., 2003. The Ireviken Event in the lower Silurian of Gotland, Sweden—relation to similar Palaeozoic and Proterozoic events. Palaeogeogr. Palaeoclimatol. Palaeoecol. 195, 99–124. https://doi.org/10.1016/S0031-0182(03)00304-3.
Munnecke, A., Calner, M., Harper, D.A., Servais, T., 2010. Ordovician and Silurian sea–water chemistry, sea level, and climate: a synopsis. Palaeogeogr. Palaeoclimatol. Palaeoecol. 296 (3–4), 389–413. https://doi.org/10.1016/j.palaeo.2010.08.001.
Nelson, N., Junge, W., 2015. Structure and energy transfer in photosystems of oxygenic photosynthesis. Annu. Rev. Biochem. 84, 659–683. https://doi.org/10.1146/annurev-biochem-092914-041942.
Norford, B.S., Orchard, M.J., 1985. Early Silurian age of rocks hosting lead-zinc mineralization at Howards Pass, Yukon Territory and District of Mackenzie: local Biostratigraphy of Road River Formation and Earn Group. Geol. Surv. Canada 83-18 (35 pp.).
Oborny, S.C., Cramer, B.D., Brett, C.E., Bancroft, A.M., 2020. Integrated Silurian conodont and carbon isotope stratigraphy of the east-central Appalachian Basin. Palaeogeogr. Palaeoclimatol. Palaeoecol. 554, 109815. https://doi.org/10.1016/j.palaeo.2020.109815.
Ostrander, C.M., Owens, J.D., Nielsen, S.G., 2017. Constraining the rate of oceanic deoxygenation leading up to a Cretaceous Oceanic Anoxic Event (OAE-2: ~94 Ma). Sci. Adv. 3 https://doi.org/10.1126/sciadv.1701020.
Owens, J.D., Gill, B.C., Jenkyns, H.C., Bates, S.M., Severmann, S., Kuypers, M.M.M., Woodfine, R.G., Lyons, T.W., 2013. Sulfur isotopes track the global extent and dynamics of euxinia during Cretaceous Oceanic Anoxic Event 2. Proc. Natl. Acad. Sci. 110, 18407–18412. https://doi.org/10.1073/pnas.1305304110.
Pagani, M., Arthur, M.A., Freeman, K.H., 1999. Miocene evolution of atmospheric carbon dioxide. Paleoceanography 14 (3), 273–292. https://doi.org/10.1029/1999PA900006.
Panchuk, K., Ridgwell, A., Kump, L.R., 2008. Sedimentary response to Paleocene-Eocene Thermal Maximum carbon release: a model-data comparison. Geology 36 (4), 315–318. https://doi.org/10.1130/G24474A.1.
Pancost, R.D., Freeman, K.H., Patzkowsky, M.E., 1999. Organic-matter source variation and the expression of a late Middle Ordovician carbon isotope excursion. Geology 27 (11), 1015–1018. https://doi.org/10.1130/0091-7613(1999)027<1015:OMSVAT>2.3.CO;2.
Patzkowsky, M.E., Slupik, L.M., Arthur, M.A., Pancost, R.D., Freeman, K.H., 1997. Late Middle Ordovician environmental change and extinction: Harbinger of the Late Ordovician or continuation of Cambrian patterns? Geology 25 (10), 911–917. https://doi.org/10.1130/0091-7613(1997)025<0911:LMOECA>2.3.CO;2.

Paytan, A., McLaughlin, K., 2007. The oceanic phosphorus cycle. Chem. Rev. 107, 563–576. https://doi.org/10.1021/cr0503613.
Penman, D.E., Zachos, J.C., 2018. New constraints on massive carbon release and recovery processes during the Paleocene-Eocene Thermal Maximum. Environ. Res. Lett. 13 (10), 105008. https://doi.org/10.1088/1748-9326/aae285.
Popp, B.N., Laws, E.A., Bidigare, R.R., Dore, J.E., Hanson, K.L., Wakeham, S.G., 1998. Effect of phytoplankton cell geometry on carbon isotopic fractionation. Geochim. Cosmochim. Acta 62, 69–77. https://doi.org/10.1016/S0016-7037(97)00333-5.
Racki, G., Baliński, A., Wrona, R., Małkowski, K., Drygant, D., Szaniawski, H., 2012. Faunal dynamics across the silurian—devonian positive isotope excursions ($\delta^{13}C$, $\delta^{18}O$) in Podolia, Ukraine: comparative analysis of the Ireviken and Klonk Events. Acta Palaeontol. Polon. 57 (4), 795–832. https://doi.org/10.4202/app.2011.0206.
Radzevičius, S., Spiridonov, A., Brazauskas, A., Norkus, A., Meidla, T., Ainsaar, L., 2014. Upper Wenlock $\delta^{13}C$ chemostratigraphy, conodont biostratigraphy and palaeoecological dynamics in the Ledai-179 drill core (Eastern Lithuania). Eston. J. Earth Sci. 63 (4), 293–299. https://doi.org/10.3176/earth.2014.33.
Rau, G.H., Riebesell, U., Wolf-Gladrow, D., 1997. CO_{2aq}-dependent photosynthetic ^{13}C fractionation in the ocean: a model versus measurements. Glob. Biogeochem. Cyc. 11, 267–278. https://doi.org/10.1029/97GB00328.
Raven, J.A., Evans, M.C.W., Korb, R.E., 1999. The role of trace metals in photosynthetic electron transport in O_2-evolving organisms. Photosynth. Res. 60, 111–150. https://doi.org/10.1023/A:1006282714942.
Raven, M.R., Fike, D.A., Gomes, M.L., Webb, S.M., Bradley, A.S., McClelland, H.-L.O., 2018. Organic carbon burial during OAE2 driven by changes in the locus of organic matter sulfurization. Nat. Commun. 9, 3409. https://doi.org/10.1038/s41467-018-05943-6.
Richardson, J.A., Keating, C., Lepland, A., Hints, O., Bradley, A.S., Fike, D.A., 2019. Silurian records of carbon and sulfur cycling from Estonia: the importance of depositional environment on isotopic trends. Earth Planet. Sci. Lett. 512, 71–82. https://doi.org/10.1016/j.epsl.2019.01.055.
Ridgwell, A., Zeebe, R.E., 2005. The role of the global carbonate cycle in the regulation and evolution of the Earth System. Earth Planet. Sci. Lett. 234, 299–315. https://doi.org/10.1016/j.epsl.2005.03.006.
Rohrssen, M.K., 2013. Molecular Organic Geochemical Records of Late Ordovician Biospheric Evolution. PhD Dissertation. University of California, Riverside, U.S.A (180 pp.).
Rose, C., Fischer, W., Finnegan, S., Fike, D., 2019. Records of carbon and sulfur cycling during the Silurian Ireviken Event in Gotland, Sweden. Geochim. Cosmochim. Acta 246, 299–316. https://doi.org/10.1016/j.gca.2018.11.030.
Saltzman, M.R., 2005. Phosphorus, nitrogen, and the redox evolution of the Paleozoic oceans. Geology 33, 573–576. https://doi.org/10.1130/G21535.1.
Saltzman, M.R., Young, S.A., Kump, L.R., Gill, B.C., Lyons, T.W., Runnegar, B., 2011. Pulse of atmospheric oxygen during the late Cambrian. Proc. Nat. Acad. Sci. 108 (10), 3876–3881. https://doi.org/10.1073/pnas.1011836108.
Samtleben, C., Munnecke, A., Bickert, T., Pätzold, J., 1996. The Silurian of Gotland (Sweden): facies interpretation based on stable isotopes in brachiopod shells. Geol. Rundsch. 85, 278–292. https://doi.org/10.1007/BF02422234.
Schachat, S.R., Labandeira, C.C., Saltzman, M.R., Cramer, B.D., Payne, J.L., Boyce, K., 2018. Phanerozoic pO_2 and the early evolution of terrestrial animals. Proc. R. Soc. B. 285 (1871), 20172631 https://doi.org/10.1098/rspb.2017.2631.
Scheller, S., Yu, H., Chadwick, G.L., McGlynn, S.E., Orphan, V.J., 2016. Artificial electron acceptors decouple archaeal methane oxidation from sulfate reduction. Science 351, 703–707. https://doi.org/10.1126/science.aad8386.
Schoffman, H., Lis, H., Shaked, Y., Keren, N., 2016. Iron-nutrient interactions within phytoplankton. Front. Plant Sci. 7, 1223. https://doi.org/10.3389/fpls.2016.01223.
Scotese, C.R., 2014. Atlas of Silurian and Middle-Late Ordovician Paleogeographic Maps (Mollweide Projection), Maps 73–80, Volume 5, The Early Paleozoic, PALEOMAP Atlas for ArcGIS, PALEOMAP Project, Evanston, IL.
Servais, T., Lehnert, O., Li, J., Mullins, G.L., Munnecke, A., Nützel, A., Vecoli, M., 2008. The Ordovician Biodiversification: revolution in the oceanic trophic chain. Lethaia 41, 99–109. https://doi.org/10.1111/j.1502-3931.2008.00115.x.
Shackleton, N.J., 1987. The carbon isotope record of the Cenozoic: history of organic carbon burial and of oxygen in the ocean and atmosphere. In: Brooks, J., Fleet, A.J. (Eds.), Marine Petroleum Source Rocks. Geological Society Special Publication, London, pp. 423–434. https://doi.org/10.1144/GSL.SP.1987.026.01.27.
Shackleton, N.J., Hall, M.A., 1984. Carbon isotope data from Leg 74 sediments. Init. Repts. DSDP 74, 613–619. https://doi.org/10.2973/dsdp.proc.74.116.1984.
Sinton, C.W., Duncon, R.A., 1997. Potential links between ocean plateau volcanism and global ocean anoxia at the Cenomanian-Turonian boundary. Econ. Geol. 92, 836–842. https://doi.org/10.2113/gseccongeo.92.7-8.836.
Smolarek, J., Trela, W., Bond, D.P., Marynowski, L., 2017. Lower Wenlock black shales in the northern Holy Cross Mountains, Poland: sedimentary and geochemical controls on the Ireviken Event in a deep marine setting. Geol. Mag. 154 (2), 247–264. https://doi.org/10.1017/S0016756815001065.
Snow, L.J., Duncan, R.A., Bralower, T.J., 2005. Trace element abundances in the Rock Canyon Anticline, Pueblo, Colorado, marine sedimentary section and their relationship to Caribbean plateau construction and oxygen anoxic event 2. Paleoceanography 20. https://doi.org/10.1029/2004PA001093.
Spero, H.J., Bijma, J., Lea, D.W., Bemis, B.E., 1997. Effect of seawater carbonate concentration on foraminiferal carbon and oxygen isotopes. Nature 390, 497–500. https://doi.org/10.1038/37333.
Štorch, P., 1994a. Graptolite biostratigraphy of the Lower Silurian (Llandovery and Wenlock) of Bohemia. Geol. J. 29, 137–165.
Štorch, P., 1994b. Llandovery-Wenlock boundary beds in the graptolite-rich sequence of the Barrandian area (Bohemia). J. Czech Geol. Soc. 39, 163–180.
Sullivan, N.B., McLaughlin, P.I., Brett, C.E., Cramer, B.D., Kleffner, M.A., Thomka, J.R., Emsbo, P., 2016. Sequence boundaries and chronostratigraphic gaps in the Llandovery of Ohio and Kentucky: the record of early Silurian paleoceanographic events in east-central North America. Geosphere 12 (6), 1813–1832. https://doi.org/10.1130/GES01343.1.
Tagliabue, A., Bowie, A.R., Boyd, P.W., Buck, K.N., Johnson, K.S., Saito, M.A., 2017. The integral role of iron in ocean biogeochemistry. Nature 543, 51–59. https://doi.org/10.1038/nature21058.
Trotter, J., Williams, I., Barnes, R., Männik, P., Simpson, A., 2016. New conodont $\delta^{18}O$ records of Silurian climate change: Implications for environmental and biological events. Palaeogeogr. Palaeoclimat. Palaeoecol. 443, 34–48. https://doi.org/10.1016/j.palaeo.2015.11.011.
Turgeon, S.C., Creaser, R.A., 2008. Cretaceous oceanic anoxic event 2 triggered by a massive magmatic episode. Nature 454, 323–329. https://doi.org/10.1038/nature07076.
Vandenbroucke, T.R., Munnecke, A., Leng, M.J., Bickert, T., Hints, O., Gelsthorpe, D., Maier, G., Servais, T., 2013. Reconstructing the environmental conditions around the Silurian Ireviken Event using carbon isotope composition of bulk and palynomorph organic matter. Geochem. Geophys. Geosyst. 14 (1), 86–101. https://doi.org/10.1029/2012GC004348.
Vandenbroucke, T.R., Emsbo, P., Munnecke, A., Nuns, N., Duponchel, L., Lepot, K., Quijada, M., Paris, F., Servais, T., Kiessling, W., 2015. Metal-induced malformations in early Palaeozoic plankton are harbingers of mass extinction. Nat. Commun. 6 (1), 1–7. https://doi.org/10.1038/ncomms8966.
Wachter, E.A., Hayes, J.M., 1985. Exchange of oxygen isotopes in carbon dioxide-phosporic acid systems. Chem. Geol. 52 (3–4), 365–374. https://doi.org/10.1016/0168-9622(85)90046-6.
Waid, C.B., Cramer, B.D., 2017. Global chronostratigraphic correlation of the Llandovery Series (Silurian System) in Iowa, USA, using high-resolution carbon isotope ($\delta^{13}C_{carb}$) chemostratigraphy and brachiopod and conodont biostratigraphy. Bull. Geosci. 92 (3), 373–390. https://doi.org/10.3140/bull.geosci.1657.
Walker, J.D., Geissman, J.W., Bowring, S.A., Babcock, L.E., 2018. Geologic Time Scale v. 5.0. Geological Society of America. https://doi.org/10.1130/2018.CTS005R3C.
Young, S.A., Kleinberg, A., Owens, J.D., 2019. Geochemical evidence for expansion of marine euxinia during an early Silurian (Llandovery–Wenlock boundary) mass extinction. Earth Planet. Sci. Lett. 513, 187–196. https://doi.org/10.1016/j.epsl.2019.02.023.
Young, S.A., Benayoun, E., Kozik, N.P., Hints, O., Martma, T., Bergström, S.M., Owens, J.D., 2020. Marine redox variability from Baltica during extinction events in the latest Ordovician-early Silurian. Palaeogeogr. Palaeoclimatol. Palaeoecol. 554, 109792. https://doi.org/10.1016/j.palaeo.2020.109792.
Zalasiewicz, J.A., Taylor, L., Rushton, A.W.A., Loydell, D.K., Rickards, R.B., Williams, M., 2009. Graptolites in British stratigraphy. Geol. Mag. 146, 785–850.